SEDIMENTOLOGY the journal of the International Association of Sedimentologists

Sedimentology (2015) **62**, 1978–2008 doi: 10.1111/sed.12214

Neoproterozoic peritidal phosphorite from the Sete Lagoas Formation (Brazil) and the Precambrian phosphorus cycle

JUSTIN B. R. DRUMMOND*[1], PEIR K. PUFAHL*, CLAUDIO G. PORTO† and MARIANA CARVALHO‡

**Department of Earth and Environmental Science, Acadia University, Wolfville, Nova Scotia, Canada B4P 2R6 (E-mail: peir.pufahl@acadiau.ca)*

†Department of Geology, Federal University of Rio de Janeiro, Rio de Janeiro, RJ, CEP 21949-900, Brazil

‡Faculty of Geology, State University of Rio de Janeiro, Rio de Janeiro, RJ, CEP 20550-900, Brazil

Associate Editor – Stephen Lokier

ABSTRACT

The Neoproterozoic Sete Lagoas Formation (*ca* 610 Ma) of the São Francisco Basin, Brazil, is a succession of siltstone, limestone and phosphorite. Phosphorite forms part of a previously unrecognized 150 to 200 m thick, unconformity bounded depositional sequence. Lithofacies stacking patterns indicate that deposition was punctuated by higher order fluctuations in base level that produced aggradational parasequences. These shallowing-upward cycles record the progradation of phosphate-rich intertidal flats over shallow subtidal deposits as accommodation filled. The presence of mudcracks, authigenic chert nodules, lack of coarse terrigenous clastics and the abundance of silt with fine, abraded quartz grains suggests accumulation along an arid coastline with significant aeolian input. Delivery of phosphorus adsorbed on aeolian Fe-(oxyhydr)oxide and clay is interpreted as having stimulated phosphogenesis in peritidal environments. Lithofacies associations indicate that windblown phosphorus promoted the establishment of cyanobacterial communities along the coast, which produced photosynthetic oxygen and the suboxic conditions necessary for the precipitation of authigenic carbonate fluorapatite. As in other Precambrian phosphatic systems, nearshore oxygen oases were a prerequisite for phosphorite accumulation because redox sensitive phosphogenic processes were pushed into the sediment to concentrate phosphorus. In more distal, anoxic environments phosphorite could not form because these biotic and abiotic processes were suspended in the water column, which cycled phosphorus in sea water rather than at the sediment–water interface. Such shallow-water phosphorite is unlike larger, younger Neoproterozoic–Phanerozoic phosphatic deposits inferred to have formed in deeper-upwelling related environments. The increasing size of phosphatic deposits through the latest Precambrian is interpreted as reflecting the progressive ventilation of the oceans during the Neoproterozoic Oxygenation Event, and resultant expansion of phosphogenic environments into distal settings. The widespread cycling of bioavailable phosphorus at the sea floor not only produced the first true phosphorite giants, but may have also been an important precondition for the evolution of multicellular animals.

[1]Present address: Department of Geological Sciences and Geological Engineering, Queen's University, Kingston, Ontario K7L 3N6, Canada.

Keywords Neoproterozoic, paragenesis, phosphorus cycle, Sete Lagoas Formation, shallow-water phosphorite.

INTRODUCTION

Phosphorite is a phosphorus-rich biochemical sedimentary rock that generally forms in association with coastal upwelling (e.g. Baturin & Bezrukov, 1979; Calvert & Price, 1983; Baturin, 1989; Glenn *et al.*, 1994; Pufahl, 2010). A true phosphorite contains a minimum of 18 wt% P_2O_5, but can have as much as 40 wt% P_2O_5, making it an important fertilizer ore (Glenn *et al.*, 1994; Trappe, 2001; Pufahl, 2010). It is also the most significant long-term sink for phosphorus (P), which regulates global biological productivity and oxygen production over geological timescales (Föllmi, 1996; Delaney, 1998; Filippelli, 2010). Thus, changes in the biogeochemical cycling of P that control phosphorite deposition also regulate the carbon cycle, climate and biological evolution (Föllmi *et al.*, 1993, 1994; Van Cappellen & Ingall, 1994, 1996; Wallmann, 2003).

Although the processes leading to the accumulation of phosphorite in the Phanerozoic are generally well-understood, the nature and significance of Precambrian phosphorite remains enigmatic (e.g. Cook & Shergold, 1990; Brasier, 1992; Nelson *et al.*, 2010). Traditionally, there has been little interest in most Precambrian deposits because they are much smaller and considered sub-economic. What is now clear, however, is that many Precambrian phosphorites do not fit the classic upwelling model, suggesting that they are very different from most in the Phanerozoic (Nelson *et al.*, 2010; Pufahl & Hiatt, 2012).

The purpose of this article is to refine what is known about Precambrian phosphorite by investigating the sedimentology, stratigraphy and petrology of phosphorite from the Neoproterozoic Sete Lagoas Formation of central Brazil (Fig. 1). The Sete Lagoas Formation is *ca* 610 Myr old (Rodrigues, 2008), and composed of siliciclastic, carbonate and phosphatic peritidal and shelf lithofacies. It accumulated during the onset of the Neoproterozoic–Cambrian Phosphogenic Episode (Cook & McElhinny, 1979; Cook & Shergold, 1990; Cook, 1992; Pufahl, 2010; Pufahl & Hiatt, 2012) which is coincident with the Neoproterozoic Oxygenation Event (Shields-Zhou & Och, 2011; Och & Shields-Zhou, 2012). The Neoproterozoic–Cambrian Phosphogenic Episode is the Earth's second major phosphatic event. Recent research suggests that it began after the Marinoan glaciation at *ca* 635 Ma and continued through the Ediacaran and Cambrian radiations of life to *ca* 510 Ma (Fig. 2; Cook, 1992; Mount & McDonald, 1992; Narbonne, 2005; Shen *et al.*, 2008; Xiao & Laflamme, 2009; Maloof *et al.*, 2010; Pufahl, 2010; Pufahl & Hiatt, 2012). The Neoproterozoic Oxygenation Event records the progressive ventilation of the deep ocean that was crucial for the evolution of multicellular animals (Narbonne, 1998, 2005, 2010; Canfield *et al.*, 2007; Shields-Zhou & Och, 2011; Och & Shields-Zhou, 2012; Zhang *et al.*, 2014).

In addition to containing an early record of these events, the Sete Lagoas Formation is important because it holds information about the nature of the benthic P cycle just prior to the deposition of the first true phosphorite giants. Phosphorite giants occur in the latest Neoproterozoic, but are generally a Phanerozoic phenomenon; they are interpreted as reflecting upwelling-related phosphorite deposition in the full spectrum of shelf environments (Nelson *et al.*, 2010; Papineau, 2010; Pufahl, 2010; Pufahl & Hiatt, 2012). The appearance of these phosphorite giants is thought to signal a transition in ocean chemistry and circulation that forever changed the biogeochemical cycling of P.

Interpreting the Sete Lagoas Formation in a sequence stratigraphic framework provides the depositional and oceanographic context critical to understanding this change. Such a backdrop is especially timely given the recent widespread application of chemical techniques to infer the depositional setting of Precambrian phosphorite (Papineau, 2010; Papineau *et al.*, 2013). These techniques are often done with little regard for the complex depositional and alteration histories that affect most Precambrian sedimentary successions (Pufahl & Hiatt, 2012).

GEOLOGICAL SETTING

The Sete Lagoas Formation is a *ca* 610 Myr old (Rodrigues, 2008; Caxito *et al.*, 2012) succession of siliciclastic, carbonate and phosphatic

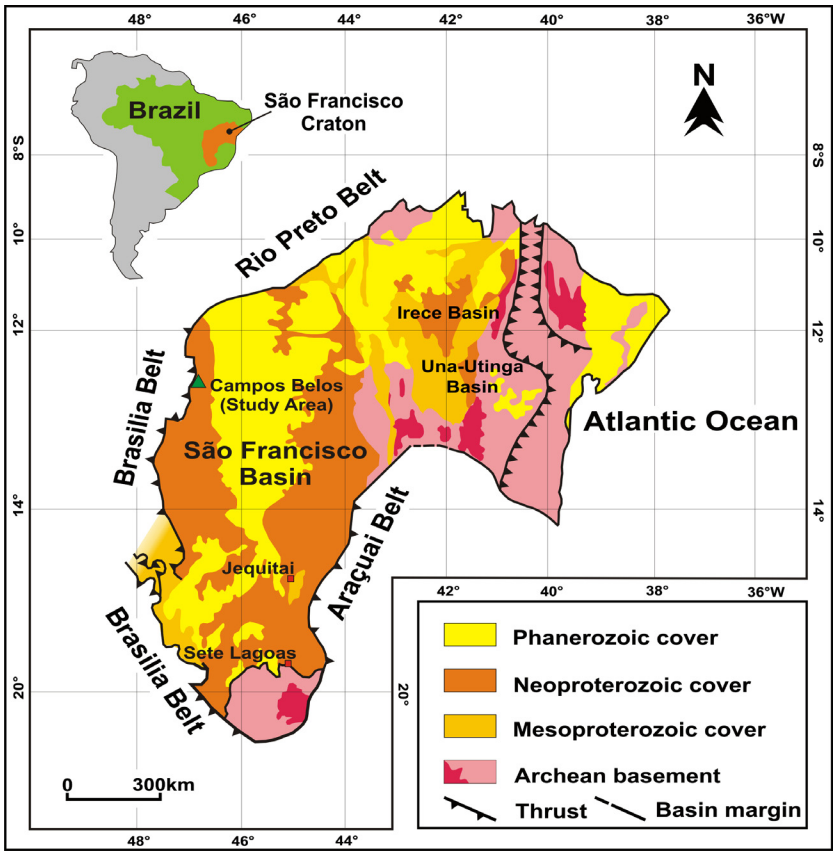

Fig. 1. Map of the São Francisco Craton showing the locations of the São Francisco Basin, the Irecê and Una-Utinga sub-basins and fold belts. Mesoproterozoic and Neoproterozoic sedimentary rocks are grouped together to form the São Francisco Supergroup. Modified after Sial *et al.* (2009).

sedimentary rocks (Martins-Neto, 2009). It is *ca* 350 m thick and is the basal unit of the Bambuí Group, which is part of the São Francisco Supergroup (Figs 1 and 3; Sial *et al.*, 2009). The São Francisco Supergroup accumulated in the São Francisco Basin, a dynamic epicratonic basin with a complex and poorly constrained tectonic history (Fig. 1; D'el-Rey Silva, 2008; Sial *et al.*, 2009). Basin fill now covers an area of *ca* 400 000 km^2 over the São Francisco Craton (Cook & Shergold, 1990; Misi & Veizer, 1998; D'el-Rey Silva, 1999, 2008; Martins-Neto *et al.*, 2001; Martins-Neto, 2009; Alkmim & Martins-Neto, 2012).

Sedimentological and structural data suggest that the São Francisco Basin began as an epeiric sea that later evolved into a foreland basin during the amalgamation of Gondwana (Alkmim *et al.*, 2001; D'el-Rey Silva, 2008; Sial *et al.*, 2009; Alkmim & Martins-Neto, 2012). Deformation associated with amalgamation first occurred along the south-western margin with the convergence of the Rio de la Plata and São Francisco cratons between *ca* 640 Ma and 620 Ma, forming the southern Brasiliano orogeny (Alkmim *et al.*, 2001). Cross-cutting relations indicate that the northern portion of the Brasilia Fold Belt formed later during convergence of the São Francisco craton with Amazonia (Alkmim *et al.*, 2001; Sial *et al.*, 2009) which deformed epeiric sea sediments of the Sete Lagaos Formation. The timing of deformation that produced the northern Brasilia belt is thought to have been coeval with the Araçuaí-West Congo orogeny. The Araçuaí-West Congo orogeny began on the eastern margin of the São Francisco craton between *ca* 625 Ma and 570 Ma (Alkmim *et al.*, 2001; Eriksson *et al.*, 2001; Pedrosa-Soares *et al.*, 2001).

Bambuí Group stratigraphy

The Neoproterozoic Bambuí Group is *ca* 2000 m thick and interpreted as having accumulated during a post-glacial transgression that formed a warm epeiric sea (Pflug & Renger, 1973; Dardenne & Walde, 1979; Dardenne *et al.*, 1986; Sial *et al.*, 2009). From base to top the Bambuí Group is formed of the Sete Lagoas Formation, the Serre da Santa Helena Formation, the Lagoa do Jacare Formation, the Serre da Saudade Formation and the Três Marias Formation (Fig. 3). These units have been grouped into three transgressive–regressive 'megacycles' (Sial *et al.*, 2009).

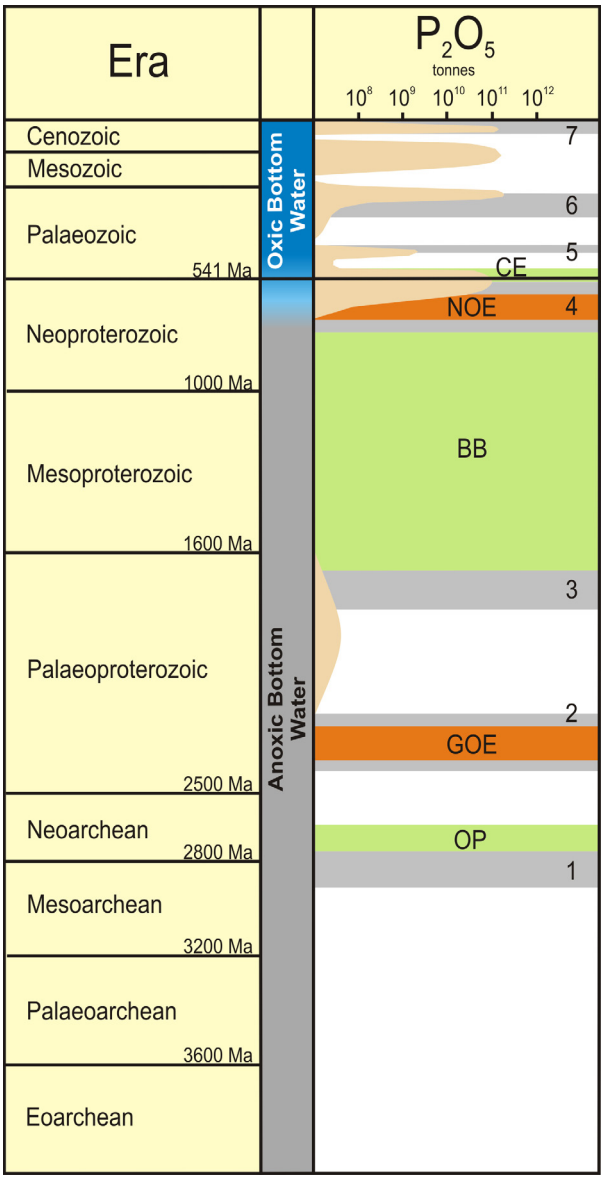

Fig. 2. Temporal distribution of phosphorite (tan curve), based on age, resource estimates and timing of Earth events in Glenn *et al.* (1994), Reddy & Evans (2009), Papineau (2010), Pufahl (2010) and Pufahl & Hiatt (2012). Events: OP = appearance of oxygenic photosynthesis; GOE = Great Oxidation Event; BB = Boring Billion; NOE = Neoproterozoic Oxygenation Event; CE = Cambrian Explosion. Glaciations: 1 = Mesoarchean; 2 = Huronian; 3 = Palaeoproterozoic; 4 = Neoproterozoic 'snowball'; 5 = Ordovician; 6 = Permian; 7 = Neogene. Modified from Pufahl & Hiatt (2012).

Megacycle I is a phosphatic siltstone-carbonate package that corresponds to the Sete Lagoas Formation. *Megacycle II* is composed of the mixed pelitic-carbonate Serra de Santa Helena Formation and overlying carbonates of the Lagoa do Jacare Formation. *Megacycle III* consists of arkosic sandstones of the Serra da Saudade Formation and the Três Marias Formation.

It is problematic that megacycles are not true depositional sequences because they include numerous, previously unrecognized unconformities (Alkmim & Martins-Neto, 2012); thus, they record varied and unrelated depositional conditions over long intervals of time. Nevertheless, seismic reflection data indicate that megacycles form an east to west thickening sedimentary wedge that is interpreted as having been shed during the Brasiliano orogeny (800 to 550 Ma; Romeiro Silva, 1997; Martins-Neto *et al.*, 2001; Martins-Neto, 2009; Alkmim & Martins-Neto, 2012).

Sete Lagoas Formation

The Sete Lagoas Formation is formed of at least three sequences. The basal sequence is characterized by folded limestone that rests unconformably on the Jequitaí Formation, a regionally recognized glacial diamictite related to the Neoproterozoic Marinoan snowball glaciation (Fig. 3; Sial *et al.*, 2009; Caxito *et al.*, 2012). A less deformed phosphatic siltstone and sandstone sequence, the focus of research herein, occurs above this limestone and forms the middle Sete Lagoas Formation (Fig. 3). The lack of correlative coarse foreland deposits and absence of synsedimentary deformation in these phosphate-rich strata suggests deposition in an epeiric sea (Cook & Shergold, 1990). Phosphatic siltstone is interbedded with lime mudstone that decreases in abundance stratigraphically upward. As the limestone diminishes there is a corresponding increase in sandstone.

This *ca* 150 to 200 m thick phosphatic succession is a true depositional sequence (e.g. Catuneanu *et al.*, 2009, 2011, 2012) with unconformable lower and upper contacts that record a complete sea-level cycle (Fig. 3). Depending on location, this succession onlaps Archean–Proterozoic gneiss, the Jequitaí Formation or folded siltstone and limestone at the base of the Sete Lagoas Formation (Dardenne *et al.*, 1986; Caxito *et al.*, 2012). Its upper contact erosionally truncates depositional facies and separates phosphatic sedimentary rocks from an overlying sequence of stromatolitic dolostone of the upper Sete Lagoas Formation (Fig. 3). Tower karst developed in this dolostone forms much of the topography in the region.

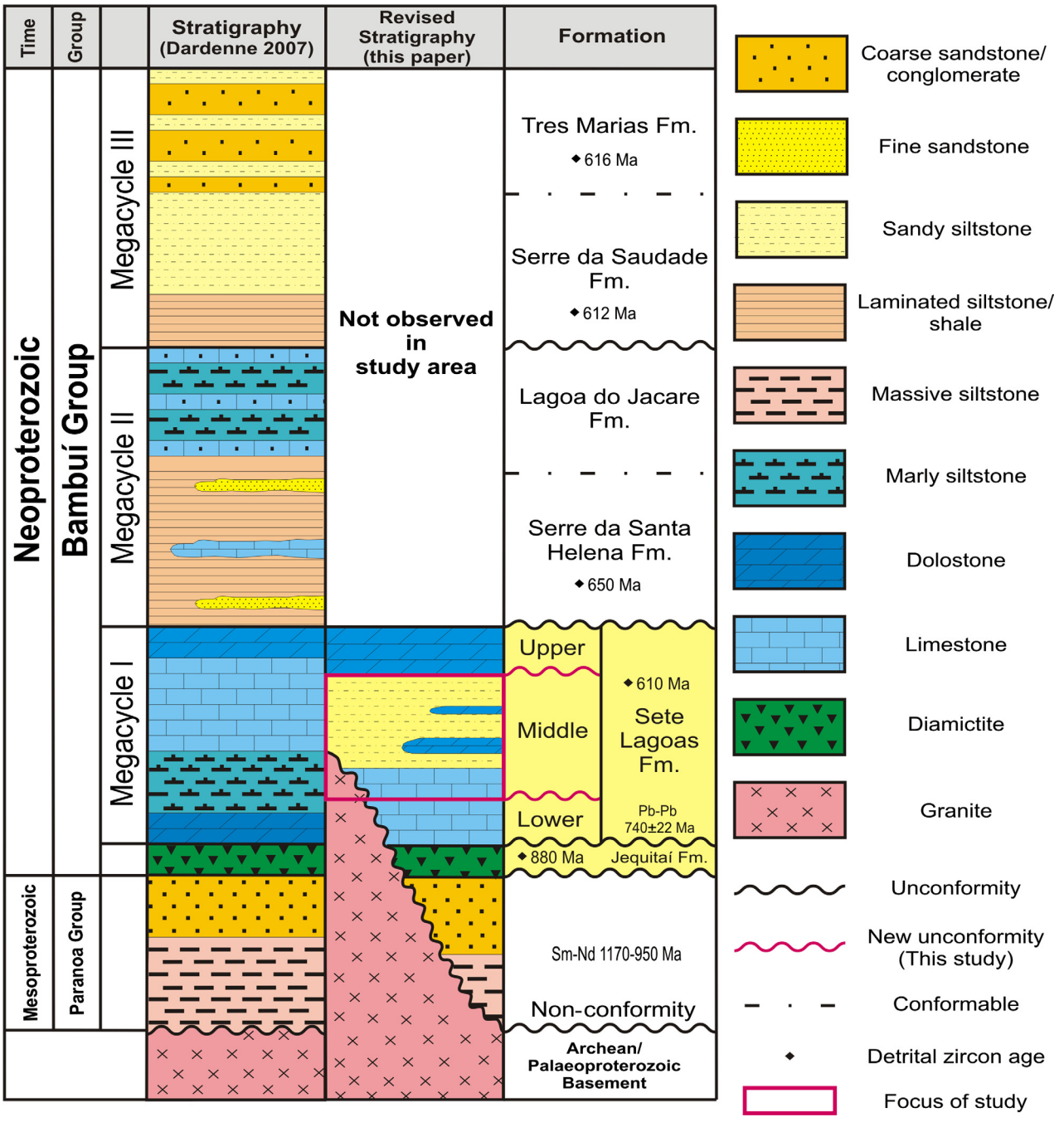

Fig. 3. Lithostratigraphic column and nomenclature of the Neoproterozoic São Francisco Supergroup as defined by Dardenne (2007) and Sial *et al.* (2009). The Sm-Nd age of Mesoproterozoic Paranoá Group is from Pimentel *et al.* (1999). The Pb-Pb age of the lower Sete Lagoas limestone is from Babinski *et al.* (2007). Youngest detrital zircon ages for the Jequitaí Formation and overlying Bambuí Group are from Rodrigues (2008).

The most robust ages of the Sete Lagoas Formation are a Pb-Pb isochron age from the basal limestone and a U-Pb detrital zircon age from the phosphatic siltstone sequence. A Pb-Pb age of 740 ± 22 Ma (Babinski *et al.*, 2007) places the deposition of the lower limestone to the middle Cryogenian and a detrital zircon age of 610 ± 15 Ma (Rodrigues, 2008) suggests deposition of phosphorite in the Ediacaran. These age relations support an early Ediacaran age for the Sete Lagoas Formation (Caxito *et al.*, 2012) and imply that phosphorite accumulation

occurred at least *ca* 20 Myr after the Marinoan snowball glaciation (Caxito *et al.*, 2012), indicating that deposition was unrelated to glacial-related changes in the P cycle.

METHODS

Because outcrops of the Sete Lagoas Formation are rare in this deeply weathered area, stratigraphic analysis was conducted primarily on drill cores. The only surface exposures investigated were in abandoned and working open pit mines operated by the MbAC Fertilizer Corporation. Outcrops contain information regarding lateral facies relations, whereas drill cores provided insight into vertical facies trends required for stratigraphic correlation. Strata are generally flat lying or gently folded; however, deformation and faulting become more prominent to the west near the Brasilia Fold Belt.

Sedimentological and stratigraphic interpretations were based on bed by bed description and sampling of five outcrop localities and 20 continuously cored drill holes (Fig. 4). Emphasis was placed on understanding palaeoenvironmental setting, regional stratigraphic trends and collection of samples for petrographic analysis. Both unweathered and weathered samples of lithofacies were collected to understand paragenesis. Percentages of chemical and clastic grains were estimated from 52 uncovered thin sections. Modal compositions were determined for grains and minerals present within each thin section using abundance indices of rare (1 to 5%), uncommon (6 to 25%), common (26 to 50%) and abundant (>50%). Thin sections were analysed using a Nikon Optiphot-Pol transmitted and reflected light microscope (Nikon Corporation, Tokyo, Japan).

Twenty thin sections were selected for polishing and additional analysis using a Nikon Eclipse E400-POL microscope equipped with a Reliotron III cathodoluminescence (CL) system (Relion Industries LLC, Bedford, MA, USA). Cathodoluminescence microfabrics provided insight into paragenetic relationships not observed using standard petrographic techniques. X-ray powder diffraction analysis of fifteen back-loaded, powdered samples confirmed lithofacies mineralogy. Samples were analysed on an X'pert-Pro Philips powder diffractometer (PANalytical BV, Almelo, The Netherlands) across scattering angles from 5° to 70° using a cobalt X-ray target source. Additional compositional information was obtained from CL spectra collected using an Ocean Optics QE65000 spectrometer (Ocean Optics Inc, Dunedin, FL, USA). This information was integrated with sedimentological and sequence stratigraphic data to develop a depositional and oceanographic model of P cycling and phosphogenesis in the Sete Lagoas Formation.

SEDIMENTOLOGY AND PALAEOENVIRONMENTS

Seven lithofacies compose the phosphatic sequence of the Sete Lagoas Formation. Bedding character and sedimentary structures indicate accumulation in peritidal to deep subtidal environments. Detailed facies descriptions are presented in Table 1. Like other Precambrian phosphorites, phosphatic facies are generally restricted to the palaeocoast (Nelson *et al.*, 2010; Pufahl & Hiatt, 2012).

Lithofacies

Peritidal lithofacies consist of phosphatic, microbial laminated mud-rich siltstone (Facies F1; Fig. 5A and B), interbedded intraclastic breccia (Facies F2; Fig. 5C) and flaser bedded quartz-rich feldspathic wacke (Facies F3; Fig. 5D). In addition to phosphate-rich microbialite, desiccation cracks (Fig. 5E), thin intraclastic grainstones and chert nodules also characterize Facies F1 (Fig. 5F). The phosphatic mineral in microbial laminae is now hydroxylapatite ($Ca_5(PO_4)_3(OH)$; Anthony *et al.*, 2000), which occurs as *in situ* peloids that grew displacively in accumulating sediment (Fig. 5B). Interbedded intraclastic grainstone beds have sharp erosive bases, are normally graded, and formed of subrounded, granule-sized to pebble-sized siltstone and microbialite intraclasts. Pebble-sized chert nodules occur as discrete layers in sediment with their long axis parallel to the plane of bedding.

Facies F2 is similar to the intraclastic grainstones in Facies F1, but intraclasts are much larger, beds are significantly thicker, and phosphatic grains are common. Angular, pebble-sized to cobble-sized intraclasts form erosive breccia beds that are 50 to 100 cm thick (Fig. 5C). Abraded hydroxylapatite grains are a common matrix constituent.

Facies F3 is primarily composed of mud draped bidirectional current ripples (Fig. 5D). Flat-topped ripples occur in muddier intervals. Planar laminated, fine-grained sandstone is common when this facies is more sand-rich. Fine quartz grains forming ripples and planar lami-

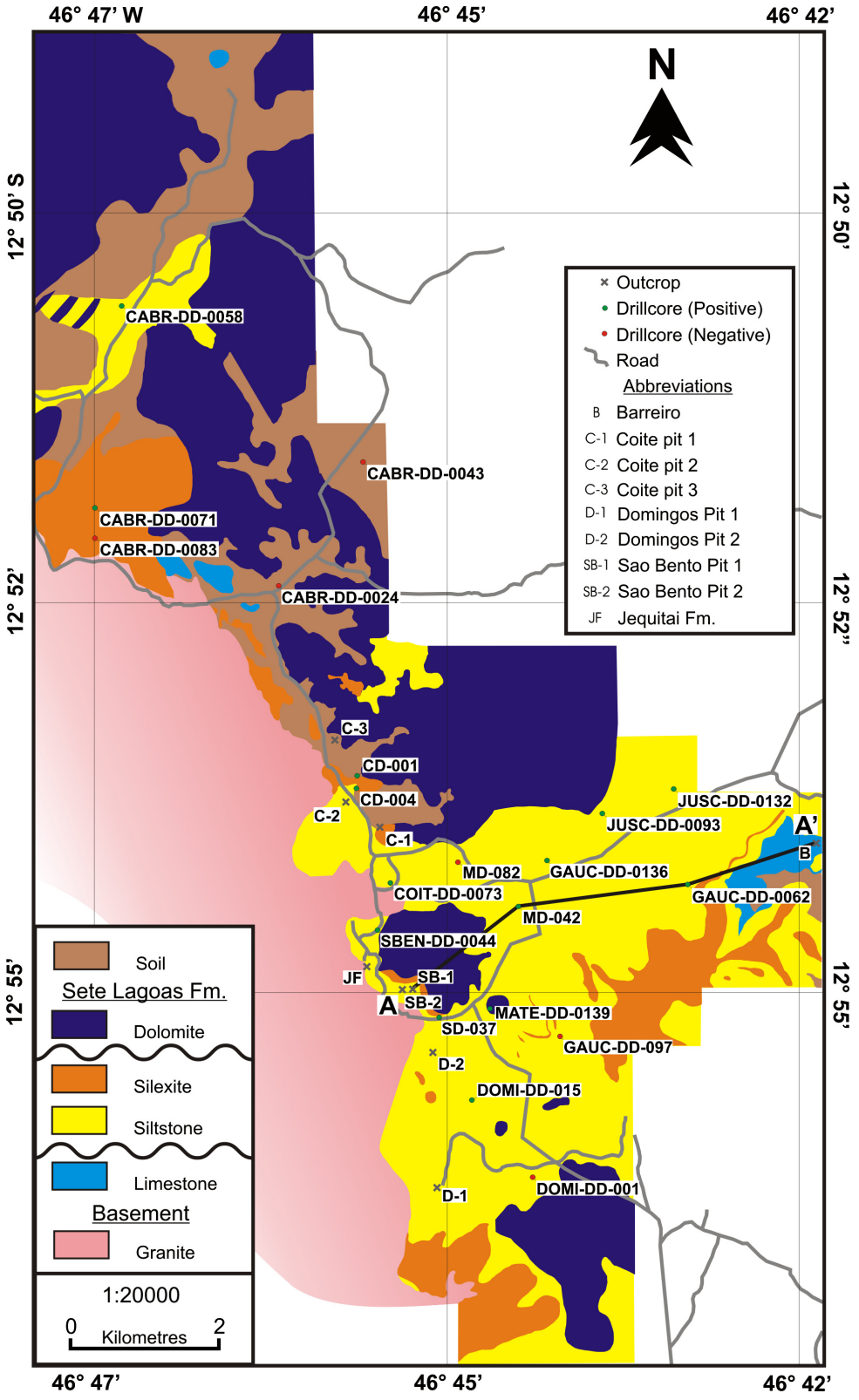

Fig. 4. Geological map of the Sete Lagoas Formation showing outcrop and drill core locations. A–A′ is the transect line for stratigraphic correlation in Fig. 9. 'Silexite' in the legend is a general term for silicified siltstone; siltstone containing abundant chert horizons and/or pedogenic silcrete.

Table 1. Lithofacies and palaeoenvironments.

	Facies	Sedimentary structures	Petrography	Interpretation
F1	Microbial laminated mud-rich siltstone	Wavy, silt-rich mudstone laminae and pustular microbial layers; desiccation cracks; Common 1 to 4 cm thick normally graded intraclastic beds containing reworked phosphatic peloids; uncommon chert nodules	Brown to dark yellow; 70 to 80% siltstone; 10 to 15% subrounded, abraded fine quartz grains; rare sucrosic dolomite, feldspar, muscovite, pyrite, dickite, wavellite; pristine and reworked phosphorite	Low to moderate-energy intertidal to supratidal mudflats and protected embayments; evaporation driven precipitation of chert and carbonate
F2	Intraclastic breccia	Poorly sorted, graded, laterally persistent beds composed of mudstone and siltstone intraclasts in matrix support; beds are 0·5 to 1 m thick and possess sharp erosive bases; can form stacked amalgamated beds	Brown to yellow; 50 to 80% angular to rounded mud and silt intraclasts; clasts range in size from granule to cobble; 20 to 30% silt matrix; rare abraded fine quartz, detrital muscovite; reworked phosphorite grains in matrix	Storm beds formed by reworking and transport of indurated peritidal sediments and pristine phosphorite
F3	Flaser bedded, quartz-rich feldspathic wacke	Well-sorted ripple cross and planar laminated sandstone and wavy laminated mudstone; 5 to 25 cm thick rippled intervals are flaser bedded with mud drapes; muddy intervals are wavy to lenticular bedded; planar laminae are millimetre-scale forming bedsets 5 to 50 cm thick; bidirectional current and flat topped ripples; rare authigenic goethite nodules	Yellow to grey-green; 30 to 40% fine abraded quartz grains; 10 to 20% fine to silt sized feldspar; 20 to 30% chlorite; uncommon muscovite, uncommon sucrosic dolomite, fracture filling calcite, subhedral hematite; rare pyrite; uncommon subhedral hematite; rare fine-grained euhedral pyrite; reworked phosphorite grains in matrix	Low to moderate energy mud-dominated intertidal mudflats and beach deposits
F4	Wavy and parallel laminated sandy siltstone	Wavy to parallel laminated siltstone with uncommon reworked francolite peloids; uncommon 1 to 4 cm thick chert beds; chert beds possess sharp tops and undulatory bases	Yellow, brown or pink; 60 to 80% siltstone; 10 to 40% mudstone; uncommon fine-grained quartz; rare muscovite and reworked phosphorite grains; chert layers are composed of replacive microcrystalline chert	Low-energy shallow subtidal setting where silt and mud accumulated via suspension settling
F5	Wavy laminated mudstone	Wavy laminated mudstone with uncommon parallel laminae; laminae have sharp lower and upper contacts	White, yellow or pink; 70 to 90% mudstone; 10 to 30% siltstone; rare fine to silt-sized quartz and muscovite	Very low-energy deep subtidal environment dominated by suspension rain

Table 1. (Continued)

	Facies	Sedimentary structures	Petrography	Interpretation
F6	Parallel and wavy bedded, silt-rich lime mudstone	Lime mudstone beds are 1 to 10 cm thick and intercalated with thin beds of rippled quartz-rich, fine sandstone; bedsets pinch out laterally over 20 to 30 m; rare, tabular 10 to 30 cm thick intraclastic rudstone beds	Grey to buff; 70 to 90% sucrosic dolomite; 10 to 20% siltstone; uncommon siltstone and lime mudstone intraclasts; rare silt-sized muscovite and angular to rounded quartz grains	Evaporative precipitation of calcium carbonate in subtidal environment with diminished clastic input
F7	Hummocky cross-stratified sandstone	Hummocky cross-stratified bedsets are 10 to 40 cm thick and pinch out laterally over 3 to 5 m; individual very fine-grained laminae are graded; thin 2 to 10 cm thick chert layers mark the top of HCS bedsets; chert layers have sharp tops and undulatory bases	Pale to dark yellow; 50 to 70% fine abraded quartz grains; 10 to 20% feldspar; uncommon detrital muscovite and reworked granular phosphorite; chert layers are composed of replacive microcrystalline chert	Storm dominated middle shelf; chert layers are siliceous hardgrounds formed during periods of quiescence associated with fair weather conditions

nae are subangular, dull and pitted in thin section.

Subtidal lithofacies include wavy and parallel laminated sandy siltstone (Facies F4; Fig. 6A), parallel and wavy laminated mudstone (Facies F5; Fig. 6B), parallel and wavy bedded, silt-rich lime mudstone (Facies F6; Fig. 6C) and hummocky cross-stratified (HCS) sandstone (Facies F7; Fig. 6D). As in peritidal facies, abraded, subangular, fine-grained quartz grains are ubiquitous (Fig. 6E and F). Granular phosphorite, current ripples and chert layers occur in all of these facies, but are most common in the phosphatic microbialite of Facies F1 and the HCS sandstone of Facies F7. Granular phosphorite laminae separate rippled layers in HCS bedsets. The tops of many bedsets are also marked by chert horizons that are 5 to 10 cm thick and have sharp upper and diffuse lower contacts.

Interpretations

Peritidal lithofacies are the phosphorite factory. The microbial laminated siltstone of Facies F1 is interpreted as pristine phosphorite recording the precipitation of what was prior to alteration sedimentary apatite, or francolite ($Ca_{10\text{-}a\text{-}b}Na_aMg_b(PO_4)_{6\text{-}x}(CO_3)_{x\text{-}y\text{-}z}(CO_3.F)_{x\text{-}y\text{-}z}(SO_4)_zF_2$; Jarvis *et al.*, 1994) in tidal flat deposits. The presence of mudcracks, flat-topped ripples and chert nodules suggests that aridity and periodic emergence promoted the evaporitic concentration of silica along the palaeocoast. Sea water was near silica saturation through most of the Neoproterozoic because of the lack of silica-secreting eukaryotes (Maliva *et al.*, 2005). Thus, evaporation probably enhanced the precipitation of opal-A, a hydrated amorphous silica precursor to chert, in peritidal environments (Maliva *et al.*, 2005; Pufahl, 2010; Akin *et al.*, 2013).

Interbedded intraclastic breccias characterizing Facies F2 are interpreted as the product of storm reworking Facies F1. Abraded hydroxylapatite grains were also probably derived from the winnowing and redeposition of authigenic francolite peloids from this pristine phosphorite.

The flaser bedded sandstones of Facies F3 record the fluctuating hydraulic conditions of tides (Reineck & Singh, 1980; Davis & Dalrymple, 2011). Planar laminated intervals probably reflect deposition on a low energy beach face at the seaward edge of the tidal flat (Schwartz, 1982; Plint, 2010). The petrographic characteristics of quartz grains composing ripples and laminae infer an aeolian source. Grains are dull and

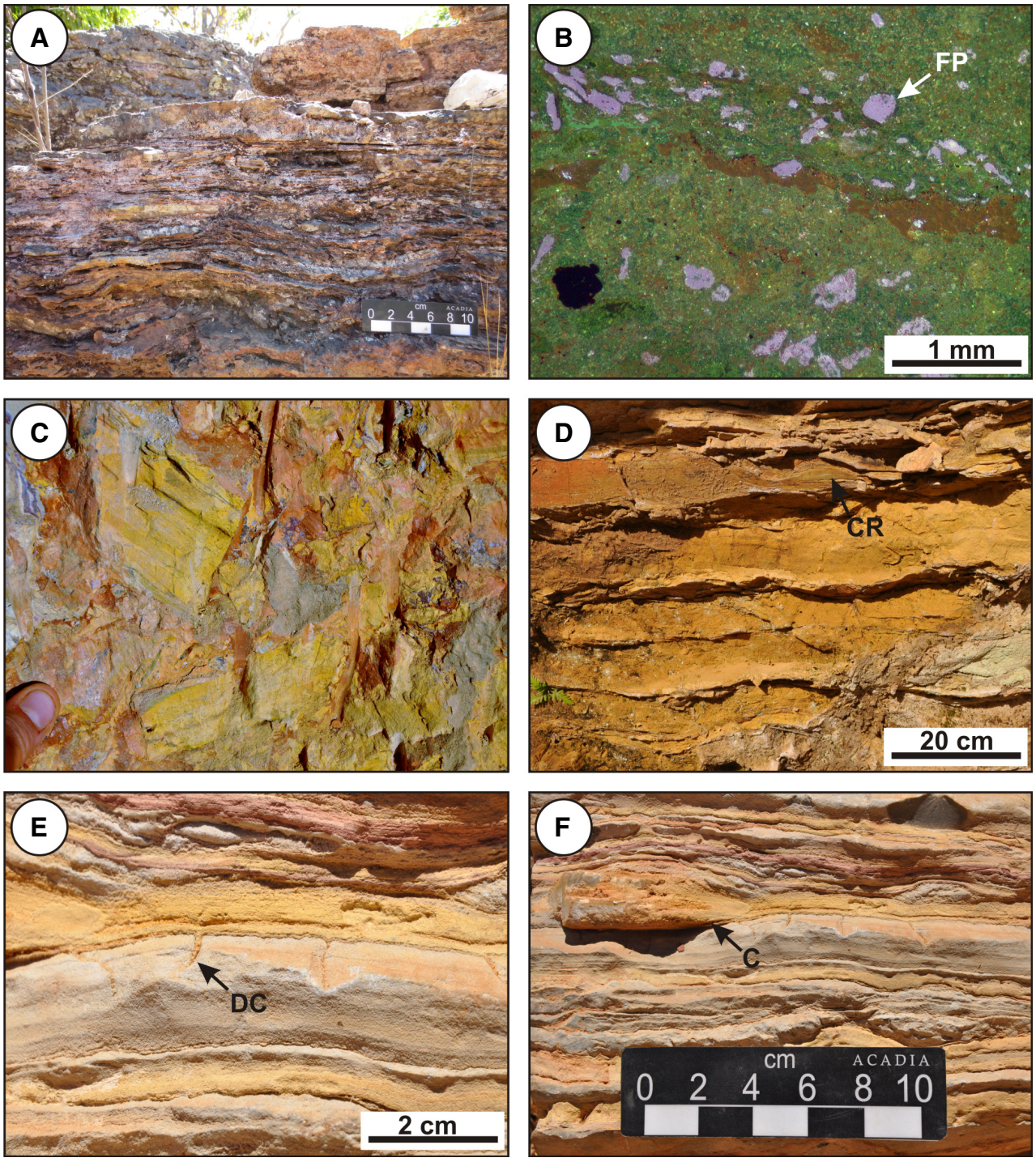

Fig. 5. (A) Pristine phosphorite formed of microbial laminated mud-rich siltstone (Facies F1). (B) *In situ* francolite peloids (FP) in pristine phosphorite occurring along microbial laminae (Facies F1; CL). (C) Intraclastic breccia that occurs interbedded with Facies F1 to F6. (D) Flaser and lenticular bedded silty sandstone (Facies F3). (E) Desiccation cracks in carbonate-rich layers (Facies 1). (F) Authigenic chert nodule (Facies 1). Compaction of layers post-dates nodule formation.

pitted from wind abrasion and more angular than those deposited subaqueously (Windom, 1975; Mazzullo *et al.*, 1986; Vandenberghe, 2013). The lack of coarse terrigenous clastics further implies that wind was the dominant transport agent of the copious fine sediment that

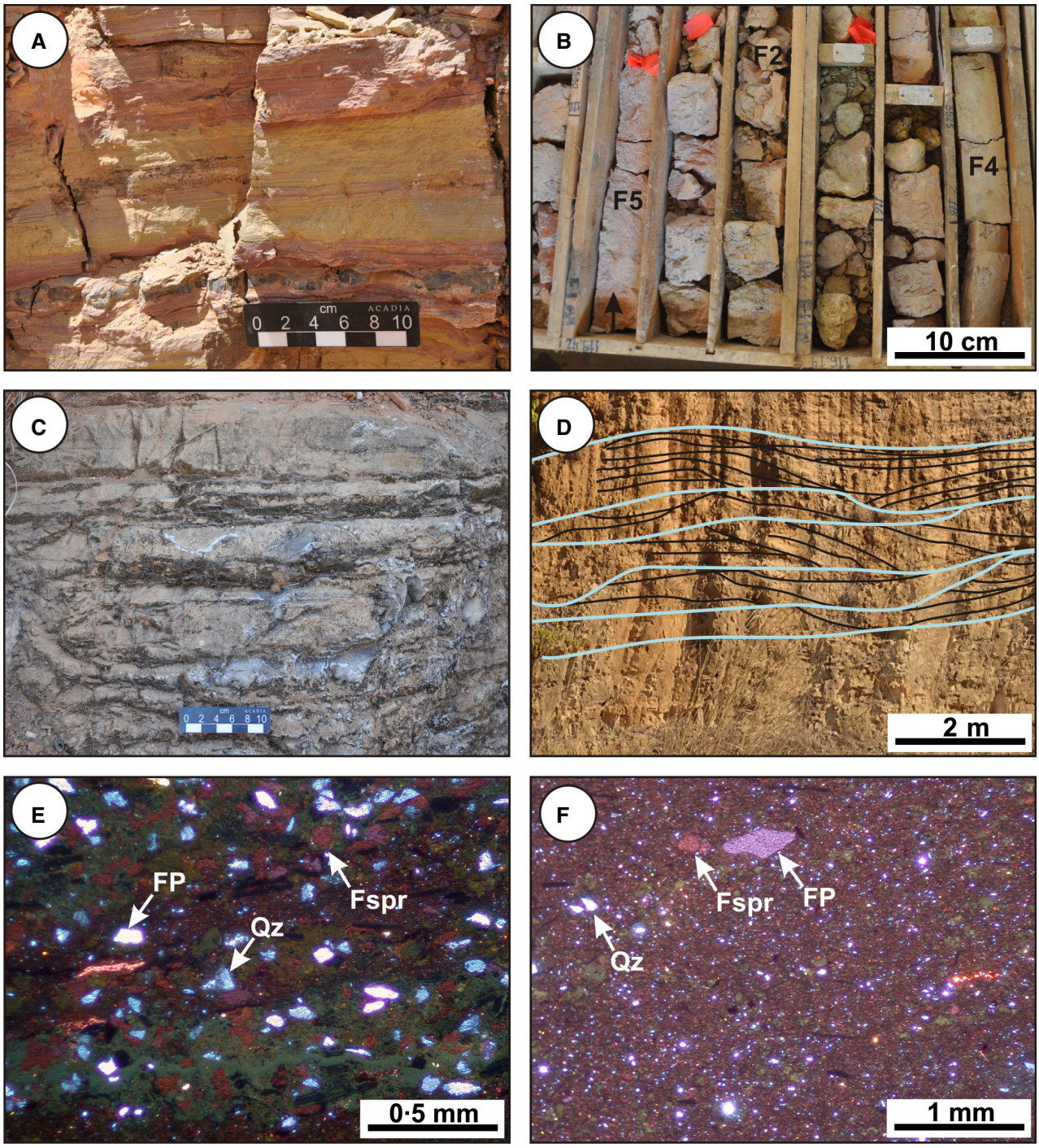

Fig. 6. (A) Wavy and parallel laminated sandy siltstone (Facies F4). Chert hardground is the dark grey layer in the lower portion of the image. (B) Parallel to wavy laminated silty mudstone (Facies F5) and interbedded wavy and parallel laminated sandy siltstone (Facies F4). Facies contacts are separated by orange marking tape. (C) Thinly bedded silty carbonate mudstone (Facies F6). (D) Hummocky cross-stratified (HCS) silty sandstone (F7). Blue lines delineate chert hardgrounds that formed at the top of HCS bedsets and black lines delineate hummocks and swales. (E) and (F) Very fine to silt-sized, angular to subrounded quartz grains (Qz; bright blue) in a silt-mud matrix (Facies 3). Feldspar (Fspr) grains are dull brown. Reworked francolite peloids (FP) are bright purple. The fine angular and pitted nature of quartz grains observed suggest that wind was the predominant transport agent. CL.

accumulated along this palaeocoast. As in many peritidal settings, the association of microbialite (Facies F1) with flaser-bedded sandstone (Facies F3) suggests that cyanobacterial mats colonized areas away from tidal currents (Decho, 2000; Lenton *et al.*, 2014).

Subtidal lithofacies primarily reflect suspension settling and storm reworking of sediment. The wavy and parallel laminated siltstone of Facies F4 is interpreted as reflecting settling of fine sediment in a calm, shallow environment above fair weather wave base, whereas the mudstone of Facies F5 implies suspension rain in a slightly deeper subtidal setting. Intervals of silt-rich lime mudstone of Facies F6 record the precipitation and suspension settling of lime mud from carbonate-saturated sea water (Tucker, 1982; Grotzinger & James, 2000; Kendall, 2010), somewhat removed from the influence of diluting siliciclastics. The presence of interbedded, current-rippled intraclastic grainstone indicates that tide and storm-generated traction currents periodically reworked a semi-lithified sea floor (Sherman *et al.*, 2000; Cozzi *et al.*, 2004; Plint, 2010).

The HCS sandstone of Facies F7 is interpreted as having accumulated in the deep subtidal of the middle shelf. Hummocky cross-stratification results from storm-generated combined flow between fair weather and storm wave-base (Dott & Bourgeois, 1982; Dumas & Arnott, 2006; Plint, 2010). Storms transported and reworked windblown sediment and authigenic francolite from peritidal environments into HCS bedsets. Granular phosphorite between rippled layers is interpreted as thin hydraulically concentrated lags produced by storm wave winnowing of redeposited sediment.

Chert horizons occurring at the top of HCS bedsets probably reflect precipitation of opal-A during fair weather conditions. Reduced delivery of terrigenous clastics between storms is thought to have allowed opal-A to concentrate and silicify the sea floor (Behl & Garrison, 1994; Maliva *et al.*, 2005; Zentmyer *et al.*, 2011). The sharp upper and diffuse lower contacts of horizons suggest that silica-saturated sea water percolated down through the sediment to precipitate opal-A (Zentmyer *et al.*, 2011) that through later diagenesis was converted to chert (Maliva *et al.*, 2005; Pufahl, 2010).

SEQUENCE STRATIGRAPHY

Lithofacies stacking patterns record a progressive deepening punctuated by higher frequency fluctuations in relative sea-level. Weathered and recycled gneiss, chert and limestone clasts from the underlying Archean–Proterozoic basement, Jequitaí diamictite and lower Sete Lagoas Formation form a transgressive lag that characterizes the basal sequence boundary. Field relations combined with recent detrital zircon data (Rodrigues, 2008; Sial *et al.*, 2009) suggest that this bounding surface represents a significant amount of missing time (Rodrigues, 2008). The profound difference in depositional style between the phosphatic siltstone sequence and overlying stromatolitic dolostones suggests that the upper bounding surface is an unconformity of similar duration.

The higher order sea-level cycles that accompanied transgression produced four preserved decametre-scale, aggradational parasequences (Figs 7 and 8). Parasequences are defined by a basal flooding surface that is generally overlain by interbedded carbonate mudstone (Facies F6), and wavy and parallel-laminated siltstone (Facies F4) that changes to flaser-bedded sandstone (Facies F3) and microbial laminated siltstone (Facies F1). These parasequences are interpreted as reflecting progradation of intertidal mudflats over subtidal deposits as accommodation filled.

Lowstand systems tract

The lowstand systems tract is 65 to 140 m thick and consists of three stacked parasequences. Parasequences 1, 2 and 3 are interpreted as recording the progressive flooding and accumulation of peritidal sediments in basement lows (Figs 7 and 8). Antecedent topography is interpreted from the presence or absence of Parasequence 1 in drill core that intersects basement (Fig. 8). Topographic highs are inferred when Parasequence 1 is absent and lows are implied when this basal parasequence is present. The calm conditions in coastal embayments created by topographic lows favoured the accumulation of windblown clay as well as the evaporative precipitation of carbonate mud.

Parasequence 1 (PS1) is 20 to 50 m thick and carbonate-rich. Carbonate mudstone (Facies F6) is interbedded with parallel-laminated sandy siltstone (Facies F4) and wavy-laminated mudstone (Facies F5). These lower subtidal deposits grade upward into intertidal microbialites (Facies F1), storm breccias (Facies F2) and tidally deposited flaser bedded sandstones (Facies F3). Lateral facies changes indi-

cate that flaser bedded sandstones accumulated between granite and limestone promontories where tide generated currents were focused and accentuated.

Parasequence 2 (PS2) is 40 to 50 m thick and similar to PS1, but contains less limestone and more wavy and parallel laminated siltstone (Facies F4). As in PS1, this shallow subtidal facies changes stratigraphically upward into intertidal flaser bedded sandstone (Facies F3) and microbialite (Facies F1). Unlike similar facies below, they contain pristine and

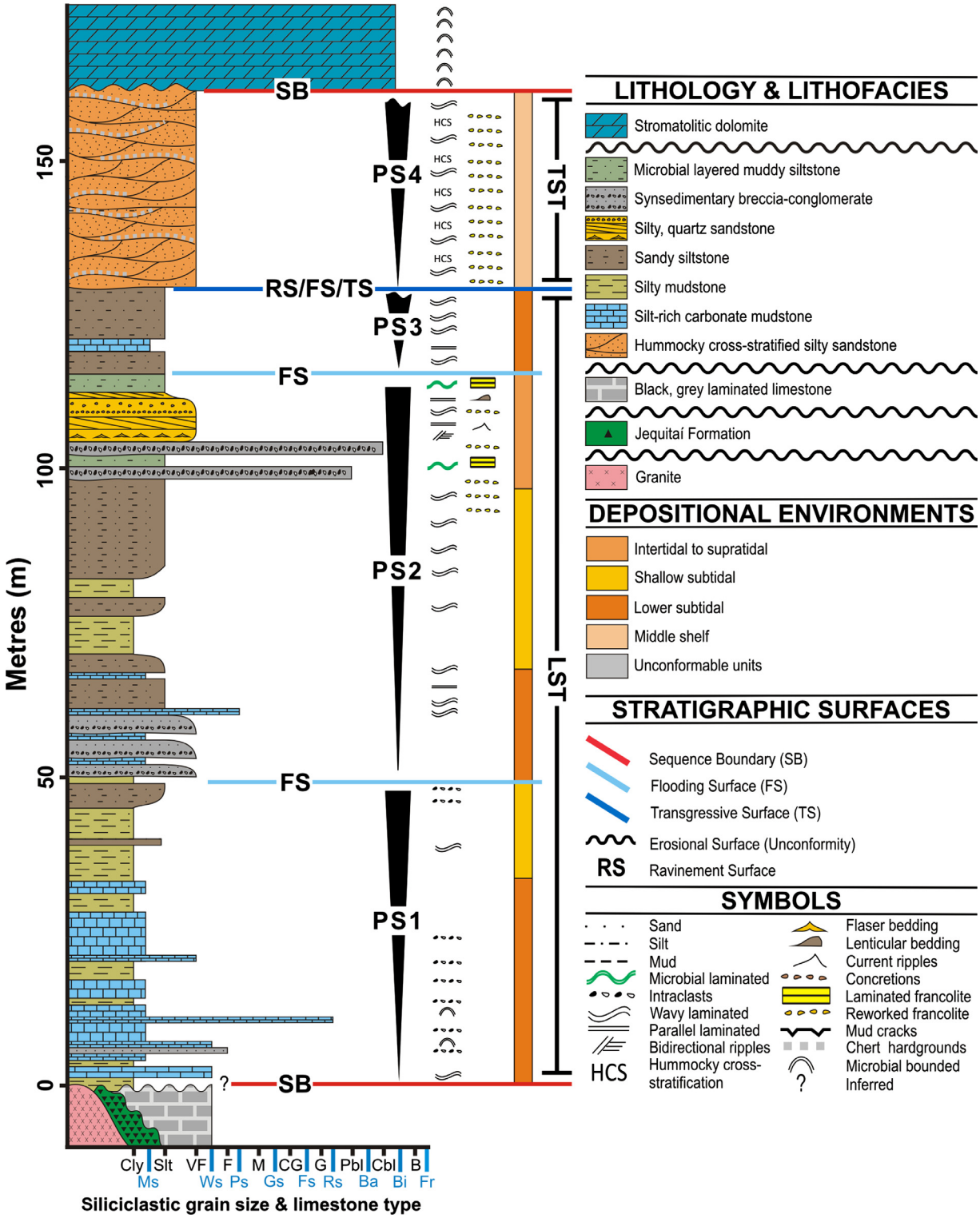

reworked phosphorite that records the progradation of phosphatic tidal flats around basement highs.

The increase of fine siliciclastics and the concomitant decrease in limestone through PS1 and PS2 indicate that aeolian-derived sediment increased through time. Such high terrigenous clastic sedimentation rates are interpreted as having diluted accumulating carbonate muds and rapidly filled available accommodation, forming expansive intertidal flats. In the early Ediacaran the São Francisco Craton was well-positioned in the subtropical high-pressure belt (Barry & Chorley, 2009) for the persistently arid conditions necessary for copious windblown sediment (Alkmim *et al.*, 2001; Powell & Pisarevsky, 2002; Li *et al.*, 2004, 2013).

Carbonate facies are rare in Parasequence 3 (PS3), which is 5 to 40 m thick and formed entirely of subtidal siltstone and mudstone (Facies F4 and F5). Intertidal facies are missing because subtidal deposits are truncated by a well-developed ravinement surface. This surface is interpreted as the transgression surface of erosion marking the inflection point between the lowstand and transgressive systems tracts (Cattaneo & Steel, 2003).

Transgressive systems tract

The transgressive systems tract is formed of one partially preserved parasequence. Parasequence 4 (PS4; Figs 7 and 8) is 30 to 60 m thick and composed entirely of HCS sandstone (F7). Much of this storm-generated middle shelf deposit is missing because of subaerial erosion prior to the deposition of the overlying stromatolitic dolostone.

DEPOSITIONAL MODEL

The Sete Lagoas Formation has traditionally been interpreted as accumulating in a foreland basin (Dardenne *et al.*, 1986; Alkmim & Martins-Neto, 2012). Such a notion, however, is not supported by stratigraphic and sedimentological data presented in this article. The unconformity-bounded sequences comprising the Sete Lagoas Formation reflect an array of depositional systems that accumulated over a protracted interval of time since the Marinoan snowball glaciation (*ca* 635 Ma). The dearth of correlative coarse siliciclastics shed during the collision of Amazonia with the São Francisco Craton, and absence of syndepositional deformation imply deposition in a basin with little tectonism. Regional seismic profiles (Martins-Neto, 2009) support this interpretation and suggest accumulation on an epeiric ramp (Burchette & Wright, 1992; Wright & Burchette, 1998). Lateral facies trends and the absence of a shelf-slope break in the Sete Lagoas Formation are consistent with a long-lived ramp that through at least three sea-level cycles produced an eastward fining and thickening sedimentary wedge.

The middle phosphatic siltstone sequence, the focus of research herein, records a phase of aridity that delivered copious aeolian sediment to the São Francisco Basin. Windblown deposits were reworked by tides and storms in inner and middle ramp settings (Fig. 9). The inner ramp is characterized by peritidal and shallow subtidal facies that includes intertidal microbial mudstone, tidally deposited flaser bedded sandstone and beach deposits (Facies F1, F2 and F3). Middle ramp deposits consist of deeper subtidal facies that accumulated via suspension rain (Facies F4, F5 and F6) or storm induced combined flow to produce HCS (Facies F7).

Unlike many Phanerozoic phosphatic systems (Glenn *et al.*, 1994; Föllmi, 1996; Pufahl, 2010), phosphogenesis was restricted to peritidal environments (Fig. 9). The lack of pristine phosphorite in deeper water settings is consistent with most other Precambrian phosphorites where upwelling was insignificant (Nelson *et al.*, 2010; Pufahl, 2010). In the Sete Lagoas Formation the precipita-

Fig. 7. Composite stratigraphic section of the phosphatic sequence in the Sete Lagoas Formation. Four aggradational parasequences are recognized. Parasequences 1, 2 and 3 comprise the lowstand systems tract (LST) and parasequence 4 forms part of the transgressive systems tract (TST). The transgressive surface (TS) is coincident with a ravinement surface (RS) and flooding surface (FS) between Parasequence 3 and 4. Parasequence 2 is the main ore horizon because it contains the highest concentration of phosphorite. Lithologies, sedimentary structures, stratigraphic surfaces and palaeoenvironmental interpretations are also used in Figs 9, 10 and 11. PS1 = parasequence 1; PS2 = parasequence 2; PS3 = parasequence 3; PS4 = parasequence 4; Cly = clay; Slt = silt; VF = very fine-grained; F = fine-grained; M = medium-grained; CG = coarse-grained; G = granule; Pbl = pebble; Cbl = Cobble; B = boulder; Ms = mudstone; Ws = wackestone; Ps; packstone; Gs = grainstone; Fs = floatstone; Rs = rudstone; Ba = bafflestone; Bi = bindstone; Fr = framestone.

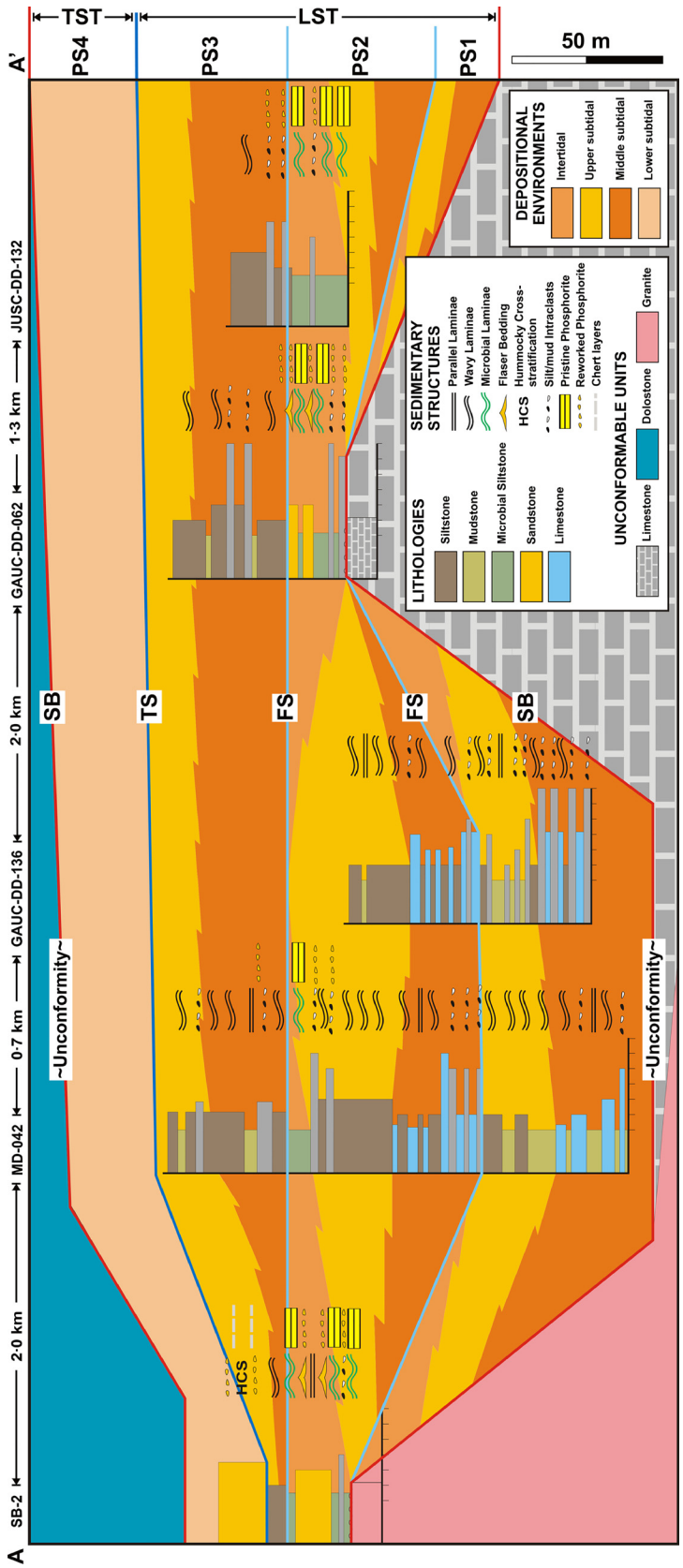

Fig. 8. Fence diagram along a transect perpendicular to the palaeoshoreline along A–A′ on Fig. 4. Datum used for correlation is the flooding surface separating PS2 and PS3.

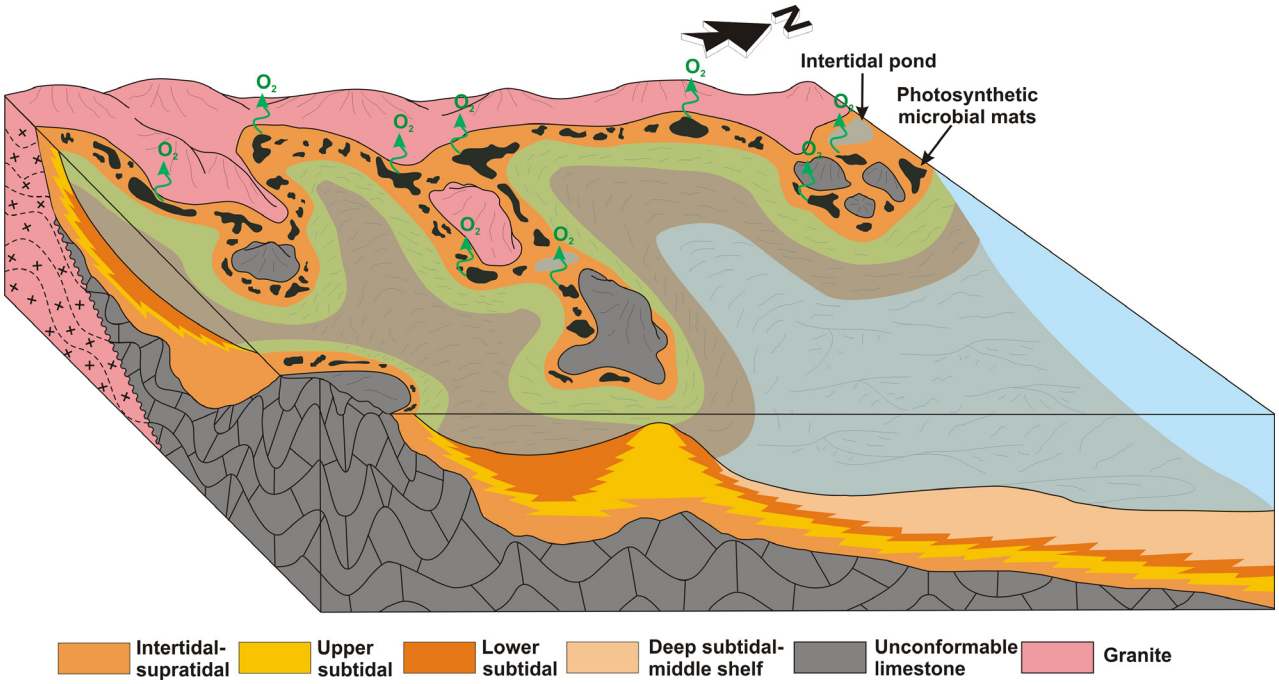

Fig. 9. Depositional model for the accumulation of the phosphatic sequence in the Sete Lagoas Formation. Intertidal–supratidal deposits are composed of Facies F1. Upper subtidal deposits are comprised of Facies F3 and F4. Lower subtidal deposits include Facies F4, F5 and F6. Middle shelf sediments are composed of Facies F7.

tion of francolite in tidal flat deposits (Facies F1) is interpreted as having been stimulated by the delivery of P adsorbed onto windblown Fe-(oxyhydr)oxides and clays (Mills *et al.*, 2004; Bünemann *et al.*, 2011; Wang *et al.*, 2012). Phosphogenesis intensified as aridity and delivery of wind-derived P increased through time. Phosphorite accumulation was greatest in PS2 when elevated aeolian input rapidly filled available accommodation to create vast intertidal flats, expanding the locus of phosphogenesis.

Low sedimentation rates and the presence of microbial mats on these windswept flats were undoubtedly important factors controlling the authigenic precipitation of francolite. Low or net negative sedimentation and the sealing effects of microbial communities would have stabilized the zone of phosphogenesis in intertidal sediment, allowing francolite to concentrate. Sedimentation rates on modern wind tidal flats vary between 1·5 and 5 cm per 100 years (Miller, 1975), which are similar to sedimentation rates in Phanerozoic, upwelling-related phosphogenic systems where stratigraphic condensation in distal environments is a prerequisite for phosphorite formation (John *et al.*, 2002); this is because tide and storm currents generally carry aeolian sediment offshore preventing accumulation in windswept coastal environments. Such bypassing of fine-grained sediment in the Sete Lagoas Formation is interpreted as having reduced sedimentation rates enough to promote phosphogenesis.

The ubiquitous presence of microbialites (Facies F1) suggests that tidal flats were colonized by cyanobacterial mats (Decho, 2000; Lenton *et al.*, 2014), similar to those characterizing modern arid intertidal environments (Walker, 1985; Hasegawa *et al.*, 2000). The ability of these mats and associated infaunal heterotrophic bacteria to fix P prevented the escape of PO_4^{3-} from the sediment and further stabilized the zone of phosphogenesis (Brasier & Callow, 2007; Callow & Brasier, 2009; Brasier *et al.*, 2010).

Also important was the production of photosynthetic oxygen by cyanobacteria, which preconditioned coastal waters for phosphogenesis (Fig. 10). The steady supply of aeolian P to peritidal environments is interpreted as having fertilized cyanobacteria, creating nearshore oxygen oases in otherwise anoxic sea water. Such oxygen enrichment would have promoted francolite precipitation by pushing redox sensitive microbial and abiotic phosphogenic processes beneath the sediment–water interface (Fig. 11; Nelson *et al.*, 2010; Pufahl & Hiatt, 2012). On an anoxic middle ramp these processes would have

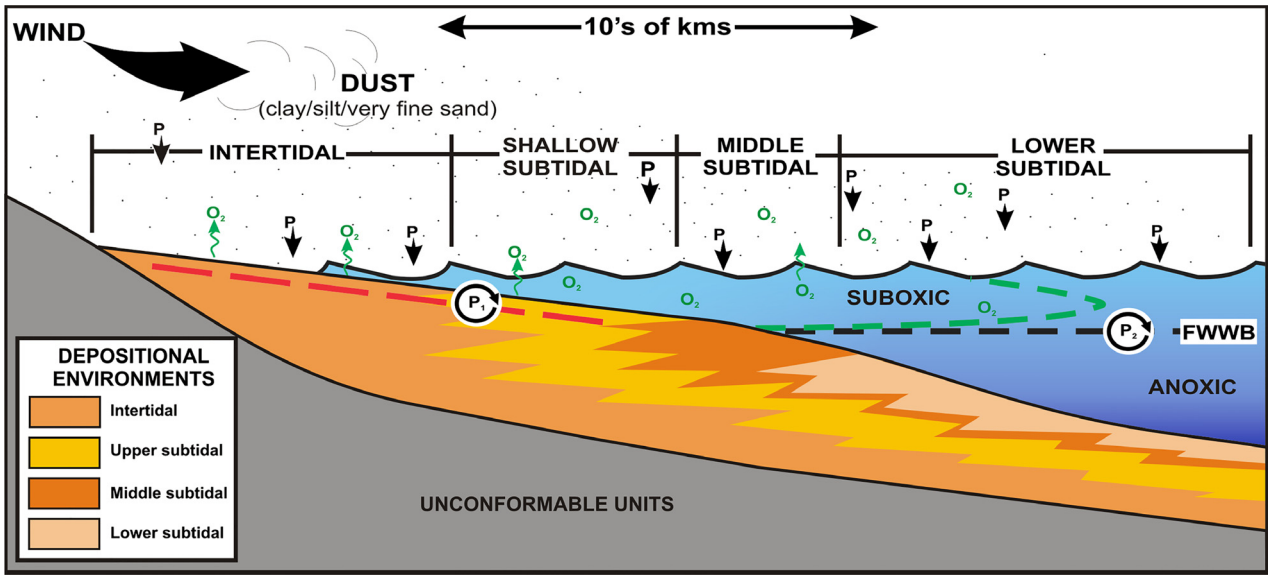

Fig. 10. Interpretation of marine redox conditions that produced peritidal phosphorite in the Sete Lagoas Formation. Aeolian processes supplied P to the coast that fertilized photosynthetic microbial communities to create oxygen oases. Suboxic conditions along the coast pushed redox sensitive phosphogenic processes (P_1) into peritidal sediments, promoting phosphogenesis (red dashed line). Anoxia in deeper settings is interpreted as having suspended P cycling in the water column (P_2), preventing phosphogenesis.

been suspended in the water column to preclude the concentration of PO_4^{3-} in sediment (Nelson *et al.*, 2010; Pufahl & Hiatt, 2012). A sluggish, anoxic middle ramp with little mixing is implied by the lack of fair weather traction deposits and the generally low oxygen conditions that are believed to have preceded ocean ventilation at 580 Ma (Canfield *et al.*, 2007; Och & Shields-Zhou, 2012).

Reworking of pristine phosphorite by tides and storms hydraulically concentrated P in peritidal environments producing granular phosphorite. These beds are much thinner and finer-grained than Phanerozoic phosphatic grainstones (e.g. Föllmi *et al.*, 1991; Grimm, 2000; Hiatt & Budd, 2001; Pufahl *et al.*, 2003). The aerially restricted nature of pristine phosphorite and lack of accommodation on the inner ramp prevented thick granular phosphorites from forming. In the Phanerozoic, stratigraphic condensation and intense reworking of large areas of upwelling-related pristine phosphorite on the middle shelf produces thick amalgamated beds of granular economic phosphorite.

ECONOMIC PHOSPHORITE

Petrographic analysis of lithofacies reveals that five paragenetic stages were involved in the formation of economic phosphorite. These are: (i) phosphogenesis and hydraulic concentration; (ii) meteoric and shallow burial diagenesis; (iii) burial diagenesis and low grade metamorphism; (iv) hydrothermal alteration and secondary phosphate mineralization; and (v) lateritization and phoscrete development (Fig. 12).

Stage 1 – Phosphogenesis and hydraulic concentration

The microbial laminated siltstone (Facies F1) is a pristine phosphorite with discontinuous phosphatic laminae and *in situ*, fine to medium sand-size, ellipsoidal peloids. Laminae and peloids are grey-brown in plane-polarized light (Fig. 13A). Laminae are concentrated in organic-rich microbial layers and peloids grew displacively with their long axes parallel to bedding. The matrix is composed of clay and abundant aeolian quartz grains (Fig. 6E and F).

Thin, tide and storm-generated granular phosphorite beds are also commonly interbedded. Beds are 1 to 4 cm thick, graded and composed of reworked phosphatic peloids in a silty matrix. In some areas storm reworking and subsequent transport produced thickly bedded intraclastic breccias (Facies F2). Breccias are formed of pebble to cobble size siltstone intraclasts in a silt-rich matrix with phosphatic

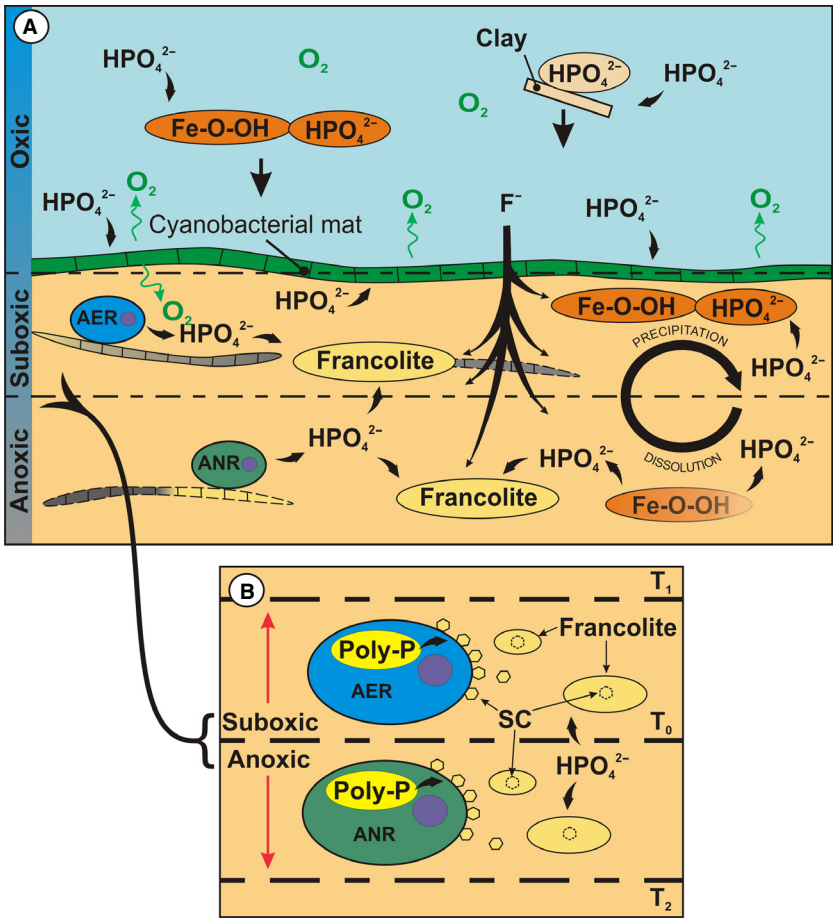

Fig. 11. Redox sensitive phosphogenic processes interpreted as having produced pristine phosphorite in peritidal settings of the Sete Lagoas Formation. The authigenic precipitation of francolite only occurred in nearshore photosynthetic oxygen oases where these processes could concentrate P beneath a suboxic sea floor (see text for discussion). (A) Delivery of P adsorbed to aeolian Fe-(oxyhydr)oxides and clays is interpreted as having fertilized photosynthetic cyanobacterial communities, stimulating oxygen production. Fe-redox cycling and bacterial respiration (bacterial oxidation and bacterial reduction) occurred in the sediment to concentrate P and precipitate authigenic francolite. (B) Microbial hydrolysis of polyphosphate (Poly-P). T_0, T_1 and T_2 depict subtle changes in the suboxic–anoxic redox boundary in the sediment profile through time. Such variability in pore water Eh may have resulted from differences in photosynthetic oxygen production in overlying sea water or changes in biological oxygen demand during organic matter degradation. During time T_0 microbes metabolize organic matter and store P within their cells as polyphosphate. Fluctuations in pore water Eh during T_1 and T_2 cause aerobic bacterial heterotrophy (AER) and anaerobic bacterial heterotrophy (ANR) to hydrolyse stored Poly-P for energy and release P pore waters. In modern environments supersaturation of HPO_4^{2-} leads to the nucleation of francolite directly on bacteria. Francolite precipitation was probably limited by the diffusion of F^- from overlying sea water.

peloids and aeolian quartz grains. Thin, storm-produced granular phosphorite beds also occur in deeper water HCS sandstone (Facies F7).

Interpretation

The association of microbialite with phosphatic laminae and *in situ* peloids suggests that phosphogenesis on tidal flats was primarily the result of microbial hydrolysis of polyphosphate and respiration of sedimentary organic matter (Fig. 11; Jarvis *et al.*, 1994; Glenn *et al.*, 2000; Soudry, 2000; Schulz & Schulz, 2005; Diaz *et al.*, 2008; Arning *et al.*, 2009a,b; Pufahl, 2010; Crosby & Bailey, 2012; Bailey *et al.*, 2013; She *et al.*, 2013). Subtle fluctuations in pore water redox chemistry may have promoted heterotrophic microbes to hydrolyse polyphosphate stored in their cells, which would have contributed PO_4^{3-} to saturate pore water (Goldhammer *et al.*, 2010; Brock & Schulz-Vogt, 2011; Crosby & Bailey, 2012). Such variability

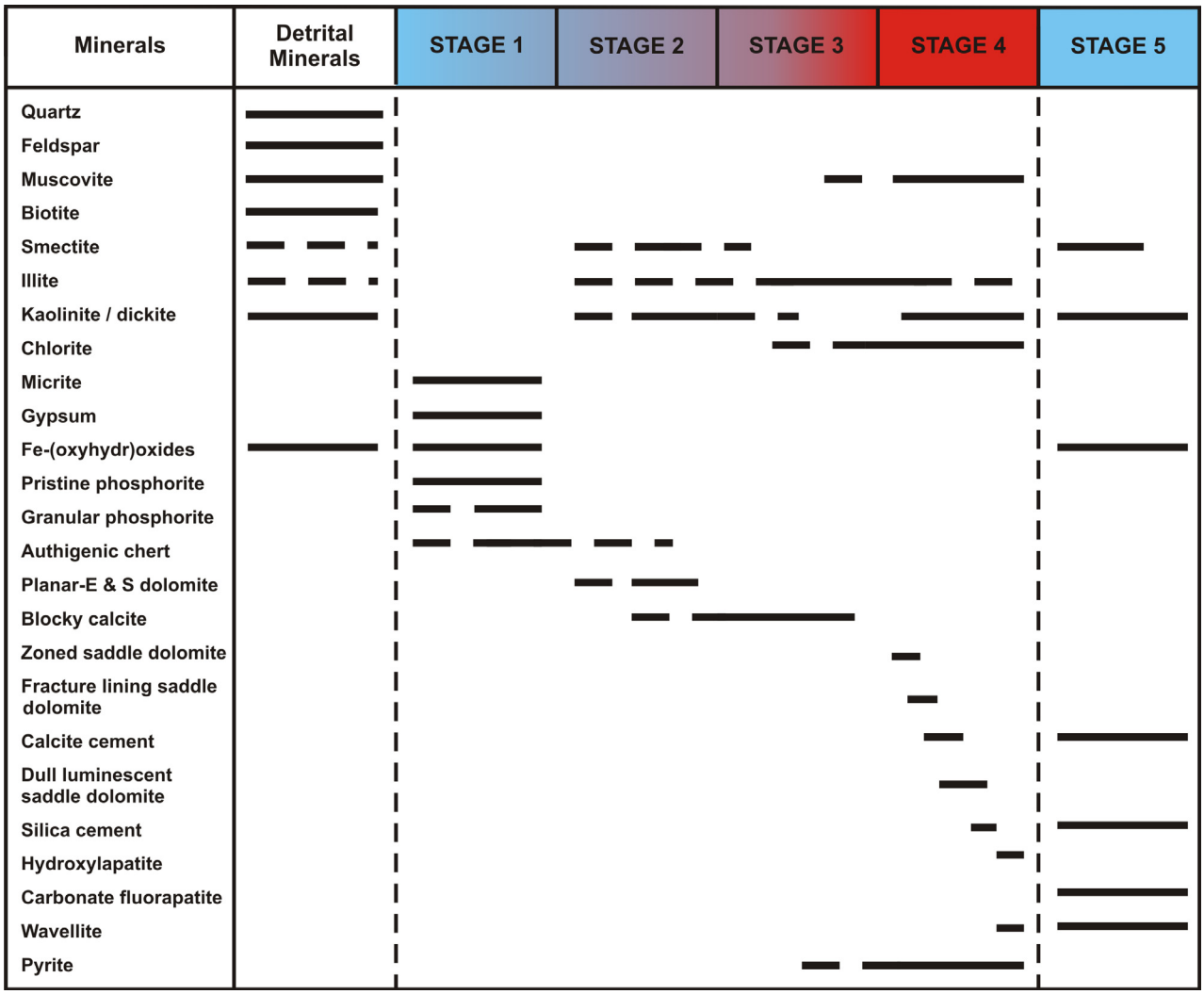

Fig. 12. Paragenesis of the phosphatic sequence in the Sete Lagoas Formation. Stage 1 = authigenesis and hydraulic reworking; Stage 2 = meteoric and shallow burial diagenesis; Stage 3 = burial diagenesis and metamorphism; Stage 4 = hydrothermal; Stage 5 = pedogenesis.

in pore water Eh could have resulted from differences in photosynthetic oxygen production in overlying sea water or changes in biological oxygen demand during organic matter degradation.

Such degradation would have also directly released P to pore water. Phosphate is liberated when organic matter is respired through a series of tiered microbially mediated redox reactions (Jarvis *et al.*, 1994; Glenn *et al.*, 2000; Soudry, 2000; Arning *et al.*, 2009a,b; Pufahl, 2010; Bailey *et al.*, 2013; She *et al.*, 2013). Of these Fe-(oxyhydr)oxide and sulphate reduction were likely to be the most important (Fig. 11). The burial, reduction and resultant dissolution of windblown Fe-(oxyhydr)oxide below the Fe redox interface would have liberated adsorbed P (Heggie *et al.*, 1990; Glenn *et al.*, 1994; Mills *et al.*, 2004; Bünemann *et al.*, 2011; Wang *et al.*, 2012). Bacterial sulphate reduction occurs slightly deeper in the sediment and is the most efficient microbial process for releasing P bound in accumulating organic matter under anoxic conditions (Arning *et al.*, 2009a). Burial of windblown clays in these anoxic pore waters would have also liberated adsorbed P for francolite precipitation (Benitez-Nelson, 2000; Bünemann *et al.*, 2011).

The escape of PO_4^{3-} from the sediment was probably prevented through its uptake by growing microbial communities or re-adsorption onto Fe-(oxyhydr)oxide just above the Fe redox

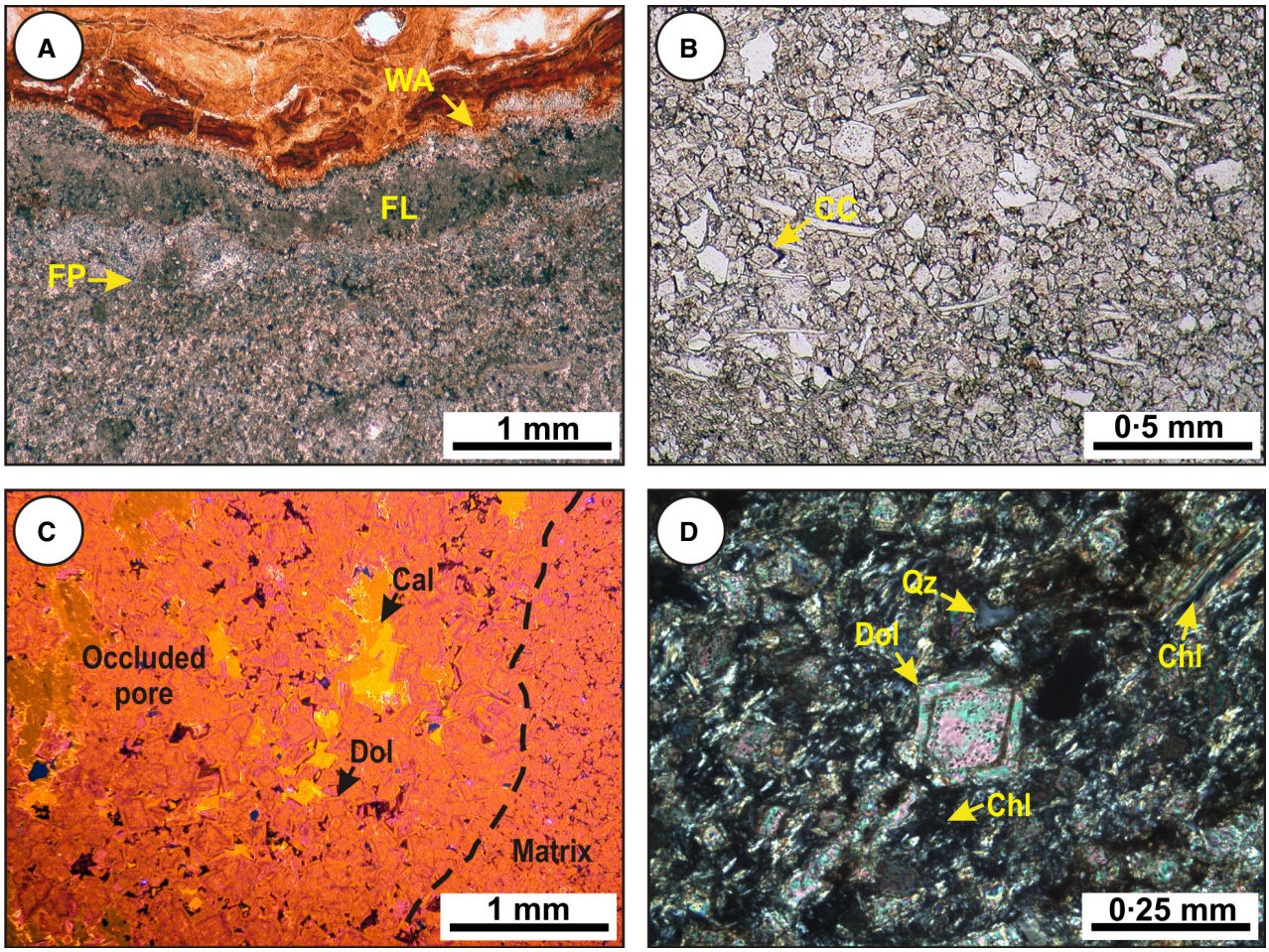

Fig. 13. (A) Pristine phosphorite composed of authigenic francolite laminae (FL) and *in situ* francolite peloids (FP; Facies F1; paragenetic stage 1). Acicular hydrothermal wavellite (WA; clear; paragenetic stage 4) lines hydrothermal fractures that are also filled with dickite (brown; paragenetic stage 4). PPL. (B) Planar-E and planar–S dolomite displaying cloudy cores (CC) and clear limpid rims (paragenetic stage 2). PPL. (C) Planar-S (matrix) dolomite and pores occluded with planar-E dolomite (Dol) and blocky calcite (Cal; Facies F6; paragenetic stage 2). CL. (D) Corroded planar-E dolomite rhomb (Dol) surrounded chlorite (Chl; Paragenetic stage 3). Qz = detrital quartz. XPL.

interface. This cyclic pumping of pore water PO_4^{3-} by Fe-(oxyhydr)oxide across the Fe redox boundary is important in Phanerozoic phosphogenic systems without upwelling (Heggie *et al.*, 1990).

Collectively, these processes defined a zone of phosphogenesis that extended only a few centimetres beneath the sea floor. The depth of this zone was regulated by the limit to which F^-, an essential element for francolite precipitation, could diffuse into the sediment from overlying sea water (Föllmi *et al.*, 1991; Jarvis *et al.*, 1994; Föllmi, 1996; Pufahl, 2010).

Once formed, pristine phosphorite was hydraulically concentrated by tides and storms to produce granular phosphorite (Facies F1 and F7). Normally graded beds were produced as storm conditions waned. The thick breccias (Facies F2) reflect storm reworking of indurated peritidal sediments and transport of intraclasts onto the tidal flat.

Stage 2 – Meteoric and shallow burial diagenesis

Pristine phosphorite (Facies F1) and associated peritidal lithofacies (Facies F3 and F6) contain sucrosic, planar-S and planar-E dolomite (Sibley & Gregg, 1987; Choquette & Hiatt, 2008). Dolomite is generally microcrystalline, except in pores where it is medium to coarsely crystalline. In pristine phosphorite (Facies F1) and flaser bedded sandstone (Facies F3) dolomite rhombs have cloudy cores and limpid rims (Fig. 13B).

Dolomite rhombs in silt-rich lime mudstone (Facies F6) are entirely clear and fabric destructive, resulting in a complete recrystallization of primary carbonate mud. Under CL, cores are non-luminescent to dully luminescent and surrounding rims are bright red-pink to red-orange in colour.

Pores in the lime mudstone (Facies F6) are rimmed by coarser planar-E dolomite or completely occluded with later blocky calcite (Fig. 13C). Blocky calcite crystals are clear under plane-polarized light and possess a homogeneous, bright orange luminescence under CL.

Interpretation

Meteoric and shallow burial diagenetic processes are interpreted as including mixing zone dolomitization and precipitation of pore-occluding, blocky calcite cement. The petrographic characteristics of dolomite in clastic lithofacies (Facies F1 and F3), cloudy cores and limpid rims with strong CL zonation, are consistent with mixing zone dolomite precipitated during meteoric diagenesis (Morad *et al.*, 1992; Boggs, 2006; Choquette & Hiatt, 2008). The entirely clear, luminescent crystals in lime mudstone (Facies F6) are characteristic of shallow burial dolomite cement (Sibley & Gregg, 1987; Choquette & Hiatt, 2008; Maliva *et al.*, 2011).

The homogeneously bright CL characteristics of pore occluding blocky calcite indicate precipitation in the shallow burial realm where pores were completely filled with fresh, persistently anoxic water (Choquette & James, 1990; Boggs, 2006). Precipitation occurred before significant compaction preserving undeformed pores.

Stage 3 – Burial diagenesis and low-grade metamorphism

X-ray diffraction confirms the presence of chlorite, muscovite $2M_1$ and illite in all siliciclastic lithofacies (Facies F1, F2, F3, F4, F5 and F7). Where these clays are most abundant, dolomite rhombs and cements are corroded (Fig. 13D). In the muddier facies (Facies F1, F4 and F5) chlorite replaces detrital biotite (Fig. 14A). Stylolites related to this paragenetic stage cross-cut all previous diagenetic fabrics and in rare instances are healed by chlorite and muscovite.

Interpretation

The co-occurrence of muscovite $2M_1$ with chlorite and illite records the breakdown of metastable detrital clays, such as smectite, montmorillonite and kaolinite, as a result of increasing temperature and pressure associated with burial (Segonzac, 1970; Bourdelle *et al.*, 2013). The association of stylolites with these clays confirms precipitation at depth during greenschist facies metamorphism.

Stage 4 – Hydrothermal alteration and secondary phosphate mineralization

X-ray powder diffraction analysis indicates that francolite in pristine (Facies F1) and reworked facies (Facies F2 and F7) was altered to hydroxylapatite ($Ca_5(PO_4)_3(OH)$), which is purple under CL (Fig. 5B). In the dolomitized lime mudstone (Facies F6) hydroxylapatite also occurs in syntaxial quartz veins and along stylolites. Wavellite ($Al_3(PO_4)_2(OH,F)_3 \cdot 5H_2O$) is the primary vein and vug-filling phosphate mineral in all clastic lithofacies (Fig. 5A). This aluminium hydroxyphosphate occurs as fracture and pore-lining acicular crystals with dickite ($Al_2Si_2O_5(OH)_4$, a high temperature polymorph of kaolinite ($Al_2Si_2O_5(OH)_4$; Ksanda & Barth, 1935). Pores generated during this paragenetic stage are non-fabric selective and range from a few millimetres to several metres across (Fig. 14B).

Saddle dolomite also fills pores and forms veins, which like those filled with hydroxylapatite and wavellite post-date stylolitization (Fig. 14C). Under CL, saddle dolomite crystals are luminescent with a light and dull red zonation (Fig. 14D). Euhedral pyrite is a common accessory mineral in all veins (Fig. 14D).

Interpretation

This diagenetic stage is characterized by the formation of late-stage porosity, hydraulic fracturing and precipitation of saddle dolomite and phosphate minerals. These hydrothermal processes were probably related to regional tectonism associated with the Brasiliano orogeny. The co-occurrence of hydroxylapatite, saddle dolomite, syntaxial quartz, chlorite, illite and muscovite $2M_1$ indicates high hydrothermal temperatures between 150°C and 300°C (Gregg, 1983; Choquette & James, 1990; Frimmel, 1997).

The association of pyrite with these minerals suggests that the composition of hydrothermal fluids was controlled primarily by thermogenic methanogenesis and sulphate reduction. Both processes decrease pore water pH encouraging

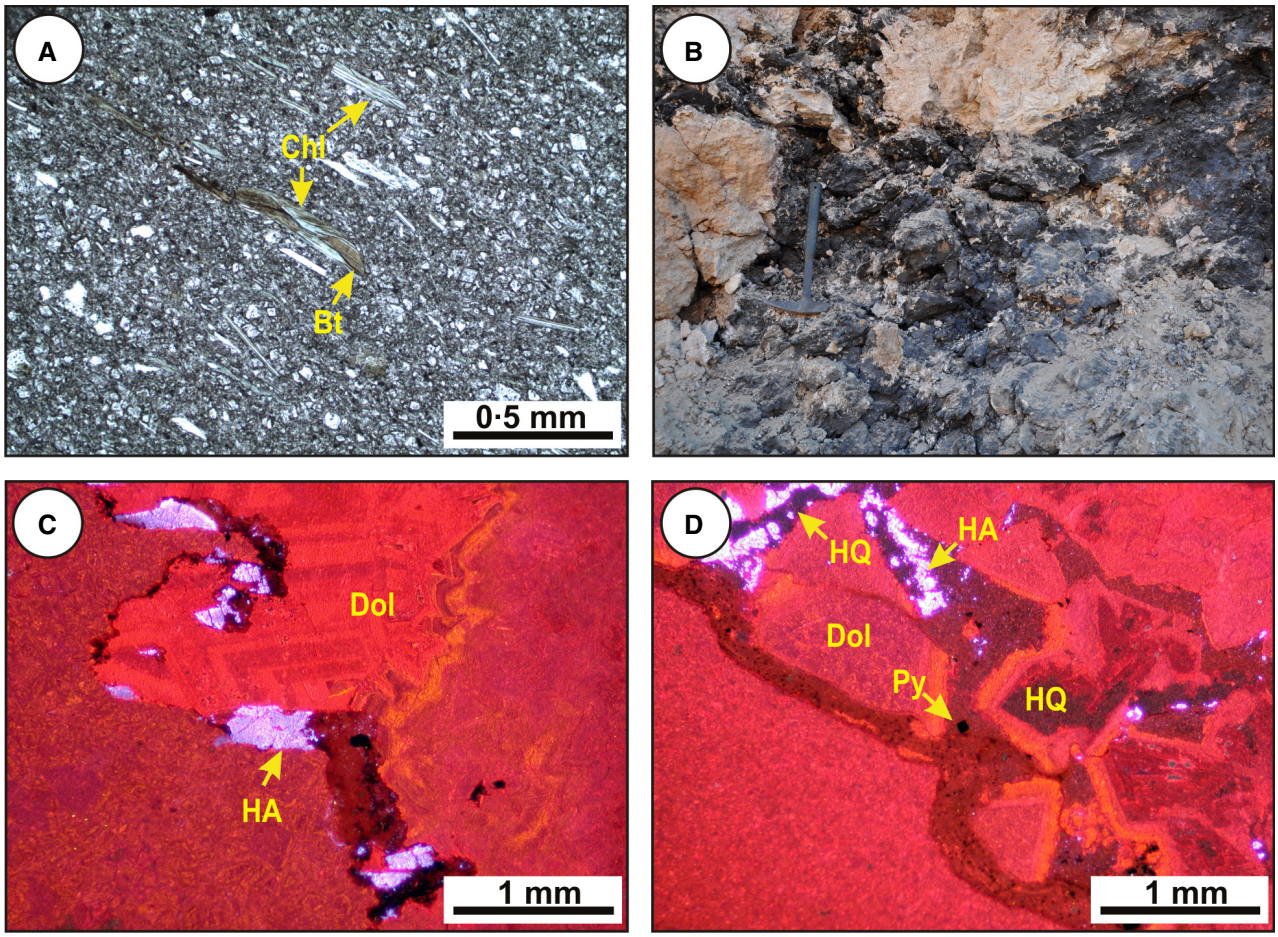

Fig. 14. (A) Chloritized detrital biotite (Bt; Chl = chlorite; paragenetic stage 3). PPL. (B) Outcrop image displaying hydrothermal dissolution cavities (paragenetic stage 4). Vugs contain wavellite stained with manganese oxide (black). Hammer for scale (34 cm in length). (C) Saddle dolomite (Dol; paragenetic stage 3) filling a dissolution pore which predates pressure dissolution. Hydroxylapatite (HA) present along stylolite (paragenetic stage 4). CL. (D) saddle dolomite (Dol) displaying corrosion and dissolution. Dissolution pores are filled with hydroxyl apatite (HA) and hydrothermal quartz (HQ) as well as minor pyrite (Py; paragenetic stage 4). CL

late porosity development and remobilization of P (Lundegard & Land, 1986; Mazzullo & Harris, 1991; Faure, 1998; Machel, 2001; Esteban & Taberner, 2003; Dolfing *et al.*, 2007). The occurrence of hydroxylapatite veins in limestone (Facies F6) indicates a concomitant increase in dissolution-related alkalinity was necessary for hyrdroxylapatite precipitation. The purple luminescence of hydroxylapatite-replaced francolite laminae and peloids implies that hydrothermal fluids were enriched in Eu^{2+} and Dy^{3+} (Boggs, 2006; Mitchell, 2014). The precipitation of wavellite and dickite in clastic lithofacies (Facies F1, F2, F3, F4, F6 and F7) was probably promoted by the dissolution of clays and detrital feldspars, which increased the concentration of $Al(OH)_3^0$ in HPO_4^{2-} rich pore waters (Vieillard & Tardy, 1984; Esteban & Taberner, 2003). The bright CL microfabrics in saddle dolomite indicate that hydrothermal fluids also contained Mn^{2+} (Gregg, 1983; Choquette & James, 1990).

Stage 5 – Lateritization and phoscrete development

Weathering and lateritization have altered the Sete Lagoas Formation to a depth of *ca* 100 m below the surface. Phoscretes only developed over phosphatic lithofacies (Facies F1, F2 and F7). A layer of younger soil now covers these duricrusts.

Phoscrete is composed of detrital quartz and clay cemented by carbonate fluorapatite, wavellite, and secondary Fe-(oxyhydr)oxides and

quartz. Carbonate fluorapatite is a coarse cavity filling cement (Fig. 15A) and wavellite lines vug walls and weathering-related fractures (Fig. 15B). Blocky quartz cement also fills pores and fractures.

Interpretation

Uplift and erosion exposed the Sete Lagoas Formation to post-burial meteoric diagenesis and Miocene lateritization (Costa, 2001; Carmo & Vasconcelos, 2004, 2006). Lateritization resulted in hydrolysis, oxidation and dissolution of detrital, authigenic, diagenetic and hydrothermal minerals. Phoscrete is interpreted as having formed under a semi-arid climate when P was liberated during the breakdown of hydroxylapatite and wavellite. Rainwater in equilibrium with the atmosphere and soil gas created meteoric waters that dissolved these minerals, liberating Ca^{2+} and PO_4^{3-} (de Keyser & Cook, 1972; Nriagu, 1976). Feldspars broke down, releasing H_4SiO_4 and producing stable clay species (Butt *et al.*, 2000). Evaporative concentration of Ca^{2+}, HPO_4^{2-} during lateritization of phosphatic lithofacies precipitated pedogenic carbonate fluorapatite ($Ca_5(PO_4,CO_3)3F$), while phosphatization of clays by P-rich groundwater produced wavellite, quartz and Fe-(oxyhydr)oxide (Nriagu, 1976; Vieillard & Tardy, 1984; Solomon & Walkden, 1985; Southgate, 1986).

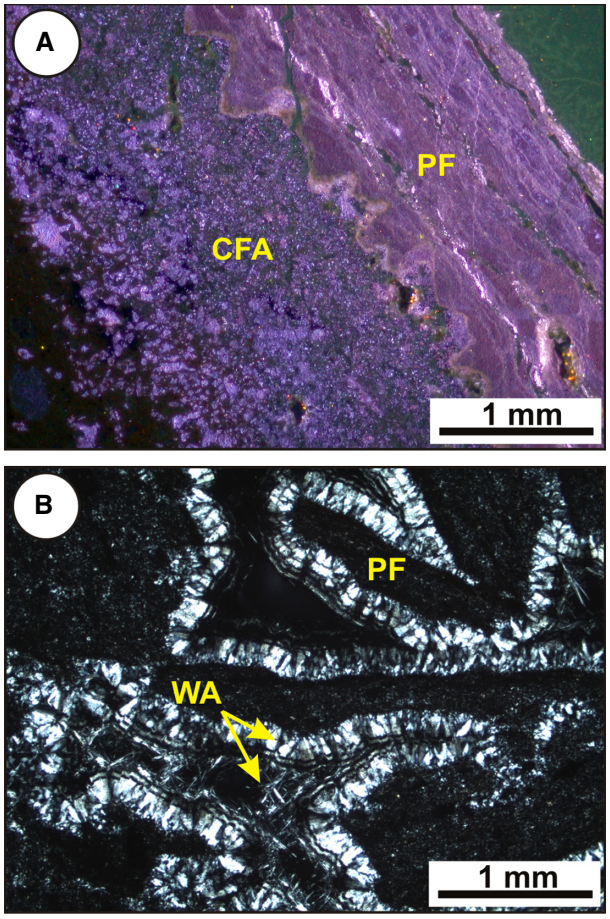

Fig. 15. (A) Pristine phosphorite intraclast (PF) in phoscrete with pedogenic carbonate fluorapatite cement (CFA; paragenetic stage 5). CL. (B) Pedogenic wavellite (WA; paragenetic stage 5) forming isopachous rinds around clasts of pristine phosphorite (PF). XPL.

Quartz cement probably formed from silica liberated during the hydrolysis of detrital feldspars and phosphatolysis of clays (Smale, 1973; Nriagu, 1976). Pedogenic Fe-(oxyhydr)oxide is interpreted as having precipitated when ferrous Fe released during pyrite oxidation, clay mineral degradation and reduction of sedimentary Fe-(oxyhydr)oxide was oxidized (Butt *et al.*, 2000). The ability of Fe-(oxyhydr)oxide to cycle and concentrate dissolved PO_4^{3-} in developing laterites was also likely to be an important phoscrete forming process (Nriagu, 1976; Arias *et al.*, 2006).

Implications

What is clear is that the Sete Lagoas Formation is paragenetically complex with several different stages of alteration related to a complicated burial and tectonic history. Pristine phosphorite formed when redox sensitive microbial and abiotic processes precipitated authigenic francolite in tidal flat sediments. Hydraulic concentration by tides and storms produced thin granular phosphorite beds. These phosphogenic and sedimentological processes produced low-grade deposits that have post-alteration concentrations of P_2O_5 averaging 4 wt%. Economic phosphorite was produced when P was remobilized from phosphatic facies by hydrothermal fluids and re-precipitated as hydroxylapatite and wavellite in veins and late-stage porosity. Such secondary precipitation of phosphatic minerals created high-grade ore with an average P_2O_5 concentration of 27 wt%. Further enrichment of P occurred where phosphatic facies and ore bodies were exposed to Miocene lateritization. Unfortunately, such a complex paragenesis has probably rendered the use of most geochemical proxies routinely employed to correlate Neoproterozoic sedimentary successions or infer palaeo-sea water history unusable (Holk *et al.*, 2003; Hiatt & Kyser, 2007; Pufahl & Hiatt, 2012).

PRECAMBRIAN PHOSPHORUS CYCLE AND BIOLOGICAL EVOLUTION

There was only one episode of phosphorite deposition that occurred completely in the Precambrian (Cook & McElhinny, 1979; Pufahl, 2010; Pufahl & Hiatt, 2012). The Palaeoproterozoic Phosphogenic Episode occurred between 2·2 Ga and 1·8 Ga, roughly coincident with the Great Oxidation Event (*ca* 2·4 to 2·0 Ga) and post-dating the Huronian glaciation (*ca* 2·45 to 2·22 Ga; Bekker & Kaufman, 2007). The conspicuous absence of Archean phosphorite (Holland, 2006; Pufahl, 2010) is interpreted as reflecting anoxic chemical weathering of P-poor primitive mafic crust (Nelson *et al.*, 2010). Such weathering produced little dissolved P, resulting in sea water with negligible bioavailable P (Nelson *et al.*, 2010; Pufahl & Hiatt, 2012). Phosphogenesis was further stifled by persistent ocean anoxia and low concentrations of sea water sulphate. Of all microbial processes, bacterial sulphate reduction most efficiently liberates P bound in accumulating organic matter (Arning *et al.*, 2009a). In the Archean, this important phosphogenic process was limited by sulphate concentrations (*ca* 200 μM to 2·4 mM; Habicht *et al.*, 2002; Poulton *et al.*, 2004) that were orders of magnitude less than in Phanerozoic sea water (Nelson *et al.*, 2010).

The appearance of phosphorite in the Palaeoproterozoic is interpreted as reflecting the change from mechanical weathering during the Huronian glaciation to chemical weathering of continental crust under an oxygenated atmosphere (Nelson *et al.*, 2010; Pufahl, 2010). The resultant delivery of P to the oceans is thought to have stimulated high surface ocean productivities, generating oxygen that contributed to the Great Oxidation Event (Papineau, 2010; Li *et al.*, 2012; Papineau *et al.*, 2013). Sedimentological data suggest that phosphogenesis was restricted to photosynthetically produced nearshore oxygen oases where authigenic francolite precipitated beneath a suboxic sea floor (Nelson *et al.*, 2010; Pufahl & Hiatt, 2012). Cessation of the Palaeoproterozoic Phosphogenic Episode is ostensibly linked to the onset of sulphidic ocean conditions (Pufahl, 2010). Through the precipitation of pyrite, such a change is interpreted as having titrated sea water of ferrous Fe (Canfield, 1998; Anbar & Knoll, 2002; Poulton *et al.*, 2004, 2010), interrupting the Fe-redox pumping of P into sediment (Nelson *et al.*, 2010; Pufahl & Hiatt, 2012). Concentration of bioavailable P by bacteria was also likely to be ineffective because redox sensitive microbial processes would have operated in the water column and not beneath the sea floor.

It was not until the Neoproterozoic that widespread euxinia waned (Shields *et al.*, 1999, 2004; Holland, 2006; Canfield *et al.*, 2007) allowing the Lazarus-like reappearance of phosphorite (Cook, 1992; Brasier & Callow, 2007; Papineau, 2010; Pufahl, 2010). As in the Palaeoproterozoic, this Neoproterozoic–Cambrian Phosphogenic Event is thought to have been stimulated by post-glacial P input (Shields, 2007; Papineau, 2010; Planavsky *et al.*, 2010). Retreat of the snowball glaciers is interpreted as having increased primary production that contributed photosynthetic oxygen to the Neoproterozoic Oxygenation Event (*ca* 800 to 550 Ma), Earth's second major oxygenation step (Papineau, 2010; Kah & Bartley, 2011; Shields-Zhou & Och, 2011; Och & Shields-Zhou, 2012; Papineau *et al.*, 2013).

The phosphatic siltstone sequence of the Sete Lagoas Formation is one of only a few Neoproterozoic phosphorites, and is thus a rare window into the nature of the P cycle during the onset of the Neoproterozoic–Cambrian Phosphogenic Event. It preserves a record of P accumulation after the Marinoan snowball glaciation, but just before the ventilation of the deep ocean at *ca* 580 Ma (Canfield *et al.*, 2007; Shen *et al.*, 2008; Och & Shields-Zhou, 2012). Similarly aged silt-rich phosphorite occurs in the Volta Basin of the West Africa craton (Trompette *et al.*, 1980; Porter *et al.*, 2004). Slightly older post-Marinoan phosphorite is found in the Irecê Basin of Brazil, which is a sub-basin of the São Franciscan Basin (Misi & Kyle, 1994; Delisle, 2015). Unlike the phosphatic siltstone sequence of the Sete Lagoas Formation this stromatolitic phosphorite rests unconformably directly on Marinoan glacial diamictites (Misi & Kyle, 1994; Misi *et al.*, 2007; Delisle, 2015). Much older Tonian to Cryogenian stromatolite-related phosphorite occurs in the Tandilia System of Argentina (Gómez-Peral *et al.*, 2014).

In the Sete Lagoas Formation the accumulation of phosphorite at least one full stratigraphic sequence above glacial diamictites suggests that increased P delivery during glacial retreat was unimportant in stimulating phosphogenesis. Instead, presented sedimentological data indicate that increasing interglacial aridity gradually raised the flux of aeolian-derived P enough for phosphorite to form. Although

stratigraphic relationships in the Irecê Basin imply a causal link between glaciation and phosphogenesis, the present work demonstrates that the P cycle through this critical interval of Earth history was more complex than previously surmised.

The occurrence of peritidal phosphorite in the Sete Lagoas Formation at *ca* 610 Ma suggests that the benthic cycling of bioavailable P was restricted to coastal oxygen oases until the ocean was fully ventilated. The deepening of the oxygen chemocline at 580 Ma (Canfield *et al.*, 2007; Shen *et al.*, 2008; Och & Shields-Zhou, 2012) coincides with increasing size of phosphatic deposits through the late Neoproterozoic. Such an expansion of phosphogenic environments allowed sequestration of upwelling-related P in the full spectrum of shelf environments, producing the first true phosphorite giants. The Doushantuo Formation in South China (*ca* 570 Ma) and temporally related phosphorite in Siberia, Kazakhstan and India record this transition (Ilyin, 1990; Brasier & Callow, 2007; Pufahl & Hiatt, 2012; Bailey *et al.*, 2013). Phosphatic lithofacies accumulated in an array of shallow water as well as in deeper, organic-rich upwelling related settings (Yueyan *et al.*, 1986; Xiao *et al.*, 1998; Jiang *et al.*, 2011).

This expansion of the locus of phosphogenesis may have initiated a negative feedback that links P and oxygen to regulate oceanic oxygen production (Van Cappellen & Ingall, 1994, 1996; Wallmann, 2003). This oxygen-P coupled response relies on the ability of Fe-redox cycling to regulate the concentration of bioavailable P at the sea floor. Phosphorus that does diffuse into the water column is important for controlling primary productivity and therefore oxygen production in the surface ocean. Once benthic P-cycling expanded into the deep ocean, this negative feedback is interpreted as having stabilized primary production and oxygen generation on a global scale. Such a process may have prevented 'runaway anoxia' during the Neoproterozoic Oxygenation Event (Van Cappellen & Ingall, 1996; Wallmann, 2003; Kah & Bartley, 2011).

Oxygen levels in the latest Neoproterozoic were probably fine-tuned through ballasting of organic matter in zooplankton faecal pellets (Porter & Robbins, 1981; Butterfield, 1997; Sperling *et al.*, 2007, 2011). The evolution of zooplankton and their ability to package C in faecal pellets is interpreted as having increased settling velocities and having reduced the consumption of oxygen in the surface ocean (Lenton *et al.*, 2014). This shifted the oxygen demand away from the surface to deeper water environments, further concentrating P in sediment (Brasier & Callow, 2007; Boyle *et al.*, 2014; Lenton *et al.*, 2014).

The Neoproterozoic Oxygenation Event not only paved the way for fully aerobic metabolisms but also forever changed the accessibility of bioavailable P at the sea floor. Prior to the Neoproterozoic Oxygenation Event, eukaryotic lineages were restricted to nearshore oxygen oases (Lenton *et al.*, 2014) where photosynthetic oxygen and bioavailable P provided a refugium for their development (Brasier & Callow, 2007; Nelson *et al.*, 2010). Consequently, the increase in abundance and diversity of multicellular animals during the Ediacaran radiation (*ca* 575 to 542 Ma) not only corresponds to the ventilation of the deep ocean (Canfield *et al.*, 2007; Shen *et al.*, 2008; Knoll, 2011; Knoll & Sperling, 2014), but also to the concomitant expansion of phosphogenic environments. This suggests that the concentration of P in benthic settings may have been an important prerequisite for the evolution of some multicellular animals, especially osmotrophs (Laflamme *et al.*, 2009). Osmotrophs survived by the passive diffusion of dissolved organic C and nutrients directly from the water column (Laflamme *et al.*, 2009; Xiao & Laflamme, 2009; Sperling *et al.*, 2011). Thus, evolution of the Ediacaran biota not only required oxygen, but probably bottom waters preconditioned with bioavailable P.

CONCLUSIONS

1 Sedimentological and stratigraphic data indicate that phosphatic sedimentary rocks in the Sete Lagoas Formation form an unconformity bounded depositional sequence. Its stratigraphic position suggests that there is no causal relationship between the Marinoan snowball glaciation and phosphogenesis.

2 Lithofacies accumulated in peritidal to middle shelf environments on an arid, evaporitic, storm-influenced epeiric ramp. Vertical and lateral stacking patterns of facies indicate that accommodation was created by an overall marine transgression punctuated by higher order fluctuations in relative sea-level. Resultant decametre-scale parasequences shallow-upward and record the progradation of variably phosphatic clastic-dominated intertidal and supratidal sediments over mixed carbonate-clastic subtidal deposits.

3 Lowstand sediments consist of three parasequences whereas the transgressive systems tract is composed of one partially preserved aggradational cycle. Highstand and falling stage deposits are missing because of post-depositional erosion. Parasequences become less carbonate and more terrigenous clastic-rich stratigraphically upward.

4 The transition from limestone to silty fine sandstone up section is interpreted as reflecting increasing aridity and aeolian input through time. The absence of upwelling-related facies and the presence of copious aeolian sediment suggest that the delivery of wind-derived P stimulated phosphogenesis along the coast.

5 Lithofacies associations indicate that phosphogenesis occurred in peritidal settings beneath photosynthetic oxygen oases, where bacterial processes and Fe-redox cycling concentrated pore water phosphate to produce pristine phosphorite. Once formed, pristine phosphorite was reworked by tides and storms and redistributed across the ramp to form granular phosphorite.

6 The Sete Lagoas Formation is paragenetically complex with several stages of alteration related to a complicated burial and tectonic history. Economic phosphorite was produced when P remobilized by hydrothermal fluids re-precipitated as hydroxylapatite and wavellite in late-stage pores and dissolution cavities.

7 The shallow nature of phosphorite in the Sete Lagoas Formation is similar to Palaeoproterozoic examples, but differs from Phanerozoic phosphogenic systems. This difference is interpreted as reflecting the dissimilarity in oxygenation state of the sea floor. The ventilation of the deep ocean at *ca* 580 Ma is thought to have pushed important redox-sensitive phosphogenic processes into progressively deeper shelf sediments, eventually allowing phosphorite to accumulate in the full spectrum of shelf environments.

8 This expansion of phosphogenic environments permitted, for the first time in Earth history, the concentration of bioavailable P in distal shelf environments. Such a change in the benthic P cycle is interpreted as having been an important precondition for the evolution and diversification of multicellular animals.

ACKNOWLEDGEMENTS

This research was funded by a Natural Sciences and Engineering Research Council of Canada Discovery Grant to Peir K. Pufahl and an Acadia Graduate Award to Justin B. R. Drummond. MbAC Fertilizer Corporation also provided funding as well as field support and access to drill core. The Geological Survey of Brazil (CPRM) provided logistical support for initial reconnaissance work. The manuscript was enriched through discussions with Eric E. Hiatt and Christa F. Koebernick. Thoughtful reviews by Karl B. Föllmi, Jake V. Bailey and Stephen W. Lokier also improved this article.

REFERENCES

Akin, S.J., **Pufahl, P.K.**, **Hiatt, E.E.** and **Pirajno, F.** (2013) Oxygenation of shallow marine environments and chemical sedimentation in Palaeoproterozoic peritidal settings: Frere Formation, Western Australia. *Sedimentology*, **60**, 1559–1582.

Alkmim, F.F. and **Martins-Neto, M.A.** (2012) Proterozoic first-order sedimentary sequences of the São Francisco craton, eastern Brazil. *Mar. Pet. Geol.*, **33**, 127–139.

Alkmim, F.F., **Marshak, S.** and **Fonseca, M.A.** (2001) Assembling West Gondwana in the Neoproterozoic: clues from the São Francisco craton region, Brazil. *Geology*, **29**, 319–322.

Anbar, A.D. and **Knoll, A.H.** (2002) Proterozoic ocean chemistry and evolution: a bioinorganic bridge? *Science*, **297**, 1137–1142.

Anthony, J.W., **Bideaux, R.A.**, **Bladh, K.W.** and **Nichols, M.C.** (2000) *Handbook of Mineralogy*, Volume 4. Mineralogical Society of America, Chantilly, Virginia, USA. Available at: http://www.handbookofmineralogy.org/

Arias, M., **Da Silva-Carballal, J.**, **García-Río, L.**, **Mejuto, J.** and **Núñez, A.** (2006) Retention of phosphorus by iron and aluminum-oxides-coated quartz particles. *J. Colloid Interf. Sci.*, **295**, 65–70.

Arning, E.T., **Birgel, D.**, **Brunner, B.** and **Peckmann, J.** (2009a) Bacterial formation of phosphatic laminites off Peru. *Geobiology*, **7**, 295–307.

Arning, E.T., **Lückge, A.**, **Breuer, C.**, **Gussone, N.**, **Birgel, D.** and **Peckmann, J.** (2009b) Genesis of phosphorite crusts off Peru. *Mar. Geol.*, **262**, 68–81.

Babinski, M., **Vieira, L.C.** and **Trindade, R.I.F.** (2007) Direct dating of the Sete Lagoas cap carbonate (Bambuí Group, Brazil) and implications for the Neoproterozoic glacial events. *Terra Nova*, **19**, 401–406.

Bailey, J.V., **Corsetti, F.A.**, **Greene, S.E.**, **Crosby, C.H.**, **Liu, P.** and **Orphan, V.J.** (2013) Filamentous sulfur bacteria preserved in modern and ancient phosphatic sediments: implications for the role of oxygen and bacteria in phosphogenesis. *Geobiology*, **11**, 397–405.

Barry, R.G. and **Chorley, R.J.** (Eds) (2009) Planetary-scale motions in the atmosphere and ocean. In: *Atmosphere, Weather and Climate*, 9th edn. pp. 163–207. Routledge, New York.

Baturin, G.N. (1989) The origin of marine phosphorites. *Int. Geol. Rev.*, **31**, 327–342.

Baturin, G.N. and **Bezrukov, P.L.** (1979) Phosphorites on the sea floor and their origin. *Mar. Geol.*, **31**, 317–332.

Behl, R.J. and **Garrison, R.E.** (1994) The origin of chert in the Monterey Formation of California (USA). In: *Siliceous, Phosphatic and Glauconitic Sediments of the Tertiary and*

Mesozoic: Proceedings of the 29th International Geological Congress, Part C (Eds A. Iijima, A.M. Abed and R.E. Garrison), pp. 101–132. A-D Druk, Zeist, The Netherlands.

Bekker, A. and **Kaufman, A.J.** (2007) Oxidative forcing of global climate change: a biogeochemical record across the oldest Palaeoproterozoic ice age in North America. *Earth Planet. Sci. Lett.*, **258**, 486–499.

Benitez-Nelson, C.R. (2000) The biogeochemical cycling of phosphorus in marine systems. *Earth Sci. Rev.*, **51**, 109–135.

Boggs, S. (2006) *Application of Cathodoluminescence Imaging to the Study of Sedimentary Rocks*. Cambridge University Press, Cambridge, 165 pp.

Bourdelle, F., **Parra, T.**, **Beyssac, O.**, **Chopin, C.** and **Vidal, O.** (2013) Clay minerals as geo-thermometer: a comparative study based on high spatial resolution analyses of illite and chlorite in Gulf Coast sandstones (Texas, U.S.A.). *Am. Mineral.*, **98**, 914–926.

Boyle, R.A., **Dahl, T.W.**, **Dale, A.W.**, **Shields-Zhou, G.A.**, **Zhu, M.**, **Brasier, M.D.**, **Canfield, D.E.** and **Lenton, T.M.** (2014) Stabilization of the coupled oxygen and phosphorus cycles by the evolution of bioturbation. *Nat. Geosci.*, **7**, 671–676.

Brasier, M.D. (1992) Palaeoceanography and changes in the biological cycling of phosphorus across the Precambrian – Cambrian boundary. In: *Origin and Early Evolution of the Metazoa* (Eds J.H. Lipps and P.W. Signor), pp. 483–523. Springer-Verlag, New York.

Brasier, M.D. and **Callow, R.H.T.** (2007) Changes in the patterns of phosphatic preservation across the Proterozoic-Cambrian transition. *Mem. Assoc. Austral. Palaeontol.*, **34**, 377–389.

Brasier, M.D., **Callow, R.H.**, **Menon, L.R.** and **Liu, A.G.** (2010) Osmotrophic biofilms: from modern to ancient. In: *Cellular Origin, Life in Extreme Habitats and Astrobiology, Microbial Mats*, Volume 14 (Eds J. Seckbach and A. Oren), pp. 131–148. Springer, New York.

Brock, J. and **Schulz-Vogt, H.N.** (2011) Sulfide induces phosphate release from polyphosphate in cultures of a marine Beggiatoa strain. *ISME J.*, **5**, 497–506.

Bünemann, E.K., Oberson, A. and Frossard, E. (Eds) (2011) *Phosphorus in Action: Biological Processes in Soil Phosphorus Cycling*. Springer, New York, USA, 483 pp.

Burchette, T.P. and **Wright, V.P.** (1992) Carbonate ramp depositional systems. *Sed. Geol.*, **79**, 3–57.

Butt, C.R., **Lintern, M.** and **Anand, R.** (2000) Evolution of regoliths and landscapes in deeply weathered terrain – implications for geochemical exploration. *Ore Geol. Rev.*, **16**, 167–183.

Butterfield, N.J. (1997) Plankton ecology and the Proterozoic-Phanerozoic transition. *Paleobiology*, **23**, 247–262.

Callow, R.H. and **Brasier, M.D.** (2009) Remarkable preservation of microbial mats in Neoproterozoic siliciclastic settings: implications for Ediacaran taphonomic models. *Earth Sci. Rev.*, **96**, 207–219.

Calvert, S.E. and **Price, N.B.** (1983) Geochemistry of Namibian shelf sediments. In: *Coastal Upwelling: Its Sedimentary Record, Part B. Sedimentary Records of Ancient Ocean Upwelling* (Eds J. Thiede and E. Seuss), pp. 337–375. Plenum Press, New York.

Canfield, D.E. (1998) A new model for Proterozoic ocean chemistry. *Nature*, **396**, 450–453.

Canfield, D.E., **Poulton, S.W.** and **Narbonne, G.M.** (2007) Late-Neoproterozoic deep-ocean oxygenation and the rise of animal life. *Science*, **315**, 92–95.

Carmo, I.O. and **Vasconcelos, P.** (2004) Geochronological evidence for pervasive Miocene weathering, Minas Gerais, Brazil. *Earth Surf. Proc. Land.*, **29**, 1303–1320.

Carmo, I.D. and **Vasconcelos, P.M.** (2006) $^{40}Ar/^{39}Ar$ geochronology constraints on late Miocene weathering rates in Minas Gerais, Brazil. *Earth Planet. Sci. Lett.*, **241**, 80–94.

Cattaneo, A. and **Steel, R.J.** (2003) Transgressive deposits: a review of their variability. *Earth Sci. Rev.*, **62**, 187–228.

Catuneanu, O., **Abreu, V.**, **Bhattacharya, J.P.**, **Blum, M.D.**, **Dalrymple, R.W.**, **Eriksson, P.G.**, **Fielding, C.R.**, **Fisher, W.L.**, **Galloway, W.E.** and **Gibling, M.R.** (2009) Towards the standardization of sequence stratigraphy. *Earth Sci. Rev.*, **92**, 1–33.

Catuneanu, O., **Galloway, W.E.**, **Kendall, C.G.S.C.**, **Miall, A.D.**, **Posamentier, H.W.**, **Strasser, A.** and **Tucker, M.E.** (2011) Sequence stratigraphy: methodology and nomenclature. *Newsl. Stratigr.*, **44**, 173–245.

Catuneanu, O., **Martins-Neto, M.A.** and **Eriksson, P.G.** (2012) Sequence stratigraphic framework and application to the Precambrian. *Mar. Pet. Geol.*, **33**, 26–33.

Caxito, F.A., **Halverson, G.P.**, **Uhlein, A.**, **Stevenson, R.**, **Gonçalves Dias, T.** and **Uhlein, G.J.** (2012) Marinoan glaciation in east central Brazil. *Precambrian Res.*, **200–203**, 38–58.

Choquette, P.W. and **Hiatt, E.E.** (2008) Shallow-burial dolomite cement: a major component of many ancient sucrosic dolomites. *Sedimentology*, **55**, 423–460.

Choquette, P.W. and **James, N.P.** (1990) Limestones—the burial diagenetic environment. In: *Diagenesis* (Eds I.A. McIlreath and D.W. Morrow), Geoscience Canada, Reprint Series, *Geol. Assoc. Canada*, **4**, 75–112.

Cook, P.J. (1992) Phosphogenesis around the Proterozoic-Phanerozoic transition. *J. Geol. Soc.*, **149**, 615–620.

Cook, P.J. and **McElhinny, M.W.** (1979) A reevaluation of the spatial and temporal distribution of sedimentary phosphate deposits in the light of plate tectonics. *Econ. Geol.*, **74**, 315–330.

Cook, P.J. and **Shergold, J.H.** (1990) *Phosphate Deposits of the World: Proterozoic and Cambrian Phosphorites*, Volume 1. Cambridge University Press, Cambridge, 408 pp.

Costa, M.L.D. (2001) The two most important lateritization cycles in the Amazon region and their paleoecological importance. *An. Acad. Brasil. Cienc.*, **73**, 461–462.

Cozzi, A., **Grotzinger, J.P.** and **Allen, P.A.** (2004) Evolution of a terminal Neoproterozoic carbonate ramp system (Buah Formation, Sultanate of Oman): effects of basement paleotopography. *Geol. Soc. Am. Bull.*, **116**, 1367–1384.

Crosby, C.H. and **Bailey, J.V.** (2012) The role of microbes in the formation of modern and ancient phosphatic mineral deposits. *Front. Microbiol.*, **3**, 241 (1–7).

Dardenne, M.A. (2007) Lithostratigraphy of the Vazante and Bambuí Groups in the São Francisco Craton and the Brasilia Fold Belt. 3rd Symposium on Neoproterozoic – Early Paleozoic Events in southwestern Gondwana, Stellenbosch, South Africa, pp. 6–8.

Dardenne, M.A. and **Walde, D.H.-G.** (1979) A estratigrafia dos Grupos Bambuí e Macaúbas no Brasil central. *Boi. Soe. Brás. Geol. Núcleo Minas Gerais*, **1**, 43–53.

Dardenne, M.A., **Trompette, R.**, **Magalhaes, L.F.** and **Scares, L.** (1986) Proterozoic and Cambrian phosphorites—regional review: Brazil. In: *Phosphate Deposits of the World, Volume 1, Proterozoic and Cambrian Phosphorites*

(Eds P.J. Cook and J.H. Shergold), pp. 116–131. Cambridge University Press, Cambridge.

Davis, R.A. and **Dalrymple, R.W.** (Eds) (2011) *Principles of Tidal Sedimentology*. Springer, New York, 636 pp.

Decho, A.W. (2000) Microbial biofilms in intertidal systems: an overview. *Cont. Shelf Res.*, **20**, 1257–1273.

Delaney, M.L. (1998) Phosphorus accumulation in marine sediments and the oceanic phosphorus cycle. *Global Biogeochem. Cycles*, **12**, 563–572.

Delisle, R.A. (2015) *Phosphatic Peritidal Limestones of the Neoproterozoic Salitre Formation, Brazil and Precambrian Economic Phosphorite*. Unpublished MSc thesis, Acadia University, 141 pp.

D'el-Rey Silva, L.J. (1999) Basin infilling in the southern-central part of the Sergipano Belt (NE Brazil) and implications for the evolution of Pan-African/Brasiliano cratons and Neoproterozoic sedimentary cover. *J. S. Am. Earth Sci.*, **12**, 453–470.

D'el-Rey Silva, L.J. (2008) Underthrusting and Late Proterozoic crustal-scale pop-up in the Brasília Belt, central Brazil. In: *1st WSEAS International Conference on Environmental and Geological Science and Engineering (EG'08), Conference Proceedings* (A. De Santis, R. Baker, B. Klug, P. Vanicek, L.J.H. D'El-Rey Silva, A. Foyo M. Ercanoglu and D. Dordevic) pp. 143–148. World Scientific and Engineering Academy Society (WSEAS) Press.

Diaz, J., **Ingall, E.**, **Benitez-Nelson, C.**, **Paterson, D.**, **de Jonge, M.D.**, **McNulty, I.** and **Brandes, J.A.** (2008) Marine polyphosphate: a key player in geologic phosphorus sequestration. *Science*, **320**, 652–655.

Dolfing, J., **Larter, S.R.** and **Head, I.M.** (2007) Thermodynamic constraints on methanogenic crude oil biodegradation. *ISME J.*, **2**, 442–452.

Dott, R.H. and **Bourgeois, J.** (1982) Hummocky stratification: significance of its variable bedding sequences. *Geol. Soc. Am. Bull.*, **93**, 663–680.

Dumas, S. and **Arnott, R.W.C.** (2006) Origin of hummocky and swaley cross-stratification—the controlling influence of unidirectional current strength and aggradation rate. *Geology*, **34**, 1073–1076.

Eriksson, P.G., **Martins-Neto, M.A.**, **Nelson, D.R.**, **Aspler, L.B.**, **Chiarenzelli, J.R.**, **Catuneanu, O.**, **Sarkar, S.**, **Altermann, W.** and **Rautenbach, C.J.W.** (2001) An introduction to Precambrian basins: their characteristics and genesis. *Sed. Geol.*, **141**, 1–35.

Esteban, M. and **Taberner, C.** (2003) Secondary porosity development during late burial in carbonate reservoirs as a result of mixing and/or cooling of brines. *J. Geochem. Explor.*, **78–79**, 355–359.

Faure, G. (1998) *Principles and Applications of Geochemistry: A Comprehensive Textbook for Geology Students*, 2nd edn. Prentice Hall, Upper Saddle River, New Jersey, 600 pp.

Filippelli, G.M. (2010) Biogeochemistry: phosphorus and the gust of fresh air. *Nature*, **467**, 1052–1053.

Föllmi, K.B. (1996) The phosphorus cycle, phosphogenesis and marine phosphate-rich deposits. *Earth Sci. Rev.*, **40**, 55–124.

Föllmi, K.B., **Garrison, R.E.** and **Grimm, K.A.** (1991) Stratification in phosphatic sediments: illustrations from the Neogene of California. In: *Cycles and Events in Stratigraphy* (Eds G. Einsele, W. Ricken and A. Seilacher), pp. 492–507. Springer-Verlag, Berlin.

Föllmi, K.B., **Weissert, H.** and **Lini, A.** (1993) Nonlinearities in phosphogenesis and phosphorus-carbon coupling and their implications for global change. In: *Interactions of C, N, P and S Biogeochemical Cycles and Global Change* (Eds R. Wollast, F.T. Mackenzie and L. Chou), *NATO ASI Ser.*, **14**, 447–474.

Föllmi, K.B., **Weissert, H.**, **Bisping, M.** and **Funk, H.** (1994) Phosphogenesis, carbon-isotope stratigraphy, and carbonate-platform evolution along the Lower Cretaceous northern Tethyan margin. *Geol. Soc. Am. Bull.*, **106**, 729–746.

Frimmel, H.E. (1997) Chlorite Thermometry in the Witwatersrand Basin: constraints on the Paleoproterozoic Geotherm in the Kaapvaal Craton, South Africa. *J. Geol.*, **105**, 601–616.

Glenn, C.R., **Follmi, K.B.**, **Riggs, S.R.**, **Baturin, G.N.**, **Grimm, K.A.**, **Trappe, J.**, **Abed, A.M.**, **Galli-Olivier, C.**, **Garrison, R.E.** and **Ilyin, A.V.** (1994) Phosphorus and phosphorites: sedimentology and environments of formation. *Eclogae Geol. Helv.*, **87**, 747–788.

Glenn, C.R., **Prévôt-Lucas, L.** and **Lucas, J.** (2000) *Marine Authigenesis: From Global to Microbial*, Vol. 66. SEPM Spec. Publ., Tulsa, Oklahoma.

Goldhammer, T., **Brüchert, V.**, **Ferdelman, T.G.** and **Zabel, M.** (2010) Microbial sequestration of phosphorus in anoxic upwelling sediments. *Nat. Geosci.*, **3**, 557–561.

Gómez-Peral, L.E., **Kaufman, A.J.** and **Poiré, D.G.** (2014) Paleoenvironmental implications of two phosphogenic events in Neoproterozoic sedimentary successions of the Tandilia System. *Precambrian Res.*, **252**, 88–106.

Gregg, J.M. (1983) On the formation and occurrence of saddle dolomite: discussion. *J. Sed. Res.*, **53**, 1025–1026.

Grimm, K.A. (2000) Stratigraphic condensation and the redeposition of economic phosphorite: allostratigraphy of Oligo-Miocene shelfal sediments, Baja California Sur, Mexico. In: *Marine Authigenesis: From Global to Microbial* (Eds C.R. Glenn, L. Prévôt-Lucas and J. Lucas), *SEPM Spec. Publ.*, **66**, 325–347.

Grotzinger, J.P. and **James, N.P.** (2000) Precambrian carbonates: evolution of understanding. In: *Carbonate Sedimentation and Diagenesis in the Evolving Precambrian World* (Eds J.P. Grotzinger and N.P. James), *SEPM Spec. Publ.*, **67**, 3–20.

Habicht, K.S., **Gade, M.**, **Thamdrup, B.**, **Berg, P.** and **Canfield, D.E.** (2002) Calibration of sulfate levels in the Archean ocean. *Science*, **298**, 2372–2374.

Hasegawa, P.M., **Bressan, R.A.**, **Zhu, J.-K.** and **Bohnert, H.J.** (2000) Plant cellular and molecular responses to high salinity. *Annu. Rev. Plant Physiol. Plant Mol. Biol.*, **51**, 463–499.

Heggie, D.T., **Skyring, G.W.**, **O'Brien, G.W.**, **Reimers, C.**, **Herczeg, A.**, **Moriarty, D.J.W.**, **Burnett, W.C.** and **Milnes, A.R.** (1990) Organic carbon cycling and modern phosphorite formation on the East Australian continental margin: an overview. *Geol. Soc. London. Spec. Publ.*, **52**, 87–117.

Hiatt, E.E. and **Budd, D.A.** (2001) Sedimentary phosphate formation in warm shallow waters: new insights into the palaeoceanography of the Permian Phosphoria Sea from analysis of phosphate oxygen isotopes. *Sed. Geol.*, **145**, 119–133.

Hiatt, E.E. and **Kyser, T.K.** (2007) Sequence stratigraphy, hydrostratigraphy, and mineralizing fluid flow in the Proterozoic Manitou Falls Formation, eastern Athabasca Basin, Saskatchewan. In: *EXTECH IV: Geology and Uranium Exploration TECHnology of the Proterozoic Athabasca Basin* (Eds C.W. Jefferson and G. Delaney), Saskatchewan and Alberta. Geological Survey of Canada,

pp. 489–506. Bulletin 588. (also Saskatchewan Geological Society Special Publication No. 18: Geological Association of Canada, Mineral Deposits Division, Special Publication No. 4).

Holk, G.J., **Kyser, T.K.**, **Chipley, D.**, **Hiatt, E.E.** and **Marlatt, J.** (2003) Mobile Pb-isotopes in Proterozoic sedimentary basins as guides for exploration of uranium deposits. *J. Geochem. Explor.*, **80**, 297–320.

Holland, H.D. (2006) The oxygenation of the atmosphere and oceans. *Phil. Trans. Roy. Soc. B Biol. Sci.*, **361**, 903–915.

Ilyin, A.V. (1990) Proterozoic supercontinent, its latest Precambrian rifting, breakup, dispersal into smaller continents, and subsidence of their margins: evidence from Asia. *Geology*, **18**, 1231–1234.

Jarvis, I., **Burnett, W.C.**, **Nathan, Y.**, **Almbaydin, F.S.M.**, **Attia, A.K.M.**, **Castro, L.N.**, **Flicoteaux, R.**, **Hilmy, M.E.**, **Husain, V.** and **Qutawnah, A.A.** (1994) Phosphorite geochemistry: state-of-the-art and environmental concerns. *Eclogae Geol. Helv.*, **87**, 643–700.

Jiang, G., **Shi, X.**, **Zhang, S.**, **Wang, Y.** and **Xiao, S.** (2011) Stratigraphy and paleogeography of the Ediacaran Doushantuo Formation (ca. 635–551 Ma) in South China. *Gondwana Res.*, **19**, 831–849.

John, C.M., **Föllmi, K.B.**, **De Kaenel, E.**, **Adatte, T.**, **Steinmann, P.** and **Badertscher, C.** (2002) Carbonaceous and phosphate-rich sediments of the Miocene Monterey Formation at El Capitan State Beach, California, U.S.A. *J. Sed. Res.*, **72**, 252–267.

Kah, L.C. and **Bartley, J.K.** (2011) Protracted oxygenation of the Proterozoic biosphere. *Int. Geol. Rev.*, **53**, 1424–1442.

Kendall, A.C. (2010) Marine evaporites. In: *Facies Models 4* (Eds N.P. James and R.W. Dalrymple), 4th ed, pp. 505–539. Geological Association of Canada, St. John's, Canada.

de Keyser, F. and **Cook, P.J.** (1972) *Geology of the Middle Cambrian Phosphorites and Associated Sediments of Northwestern Queensland*, Vol. 138. Bureau of Mineral Resources, Geology and Geophysics, Canberra.

Knoll, A.H. (2011) The multiple origins of complex multicellularity. *Annu. Rev. Earth Planet. Sci.*, **39**, 217–239.

Knoll, A.H. and **Sperling, E.A.** (2014) Oxygen and animals in earth history. *Proc. Natl Acad. Sci. USA*, **111**, 3907–3908.

Ksanda, C.J. and **Barth, T.F.** (1935) Note on the structure of dickite and other clay minerals. *Am. Mineral.*, **20**, 631–637.

Laflamme, M., **Xiao, S.** and **Kowalewski, M.** (2009) Osmotrophy in modular Ediacara organisms. *Proc. Natl Acad. Sci. USA*, **106**, 14438–14443.

Lenton, T.M., **Boyle, R.A.**, **Poulton, S.W.**, **Shields-Zhou, G.A.** and **Butterfield, N.J.** (2014) Co-evolution of eukaryotes and ocean oxygenation in the Neoproterozoic era. *Nat. Geosci.*, **7**, 257–265.

Li, Z.-X., **Evans, D.A.D.** and **Zhang, S.** (2004) A 90° spin on Rodinia: possible causal links between the Neoproterozoic supercontinent, superplume, true polar wander and low-latitude glaciation. *Earth Planet. Sci. Lett.*, **220**, 409–421.

Li, Y.-L., **Sun, S.** and **Chan, L.S.** (2012) Phosphogenesis in the 2460 and 2728 million-year-old banded iron formations as evidence for biological cycling of phosphate in the early biosphere. *Ecol. Evol.*, **3**, 115–125.

Li, Z.-X., **Evans, D.A.D.** and **Halverson, G.P.** (2013) Neoproterozoic glaciations in a revised global palaeogeography from the breakup of Rodinia to the assembly of Gondwanaland. *Sed. Geol.*, **294**, 219–232.

Lundegard, P.D. and **Land, L.S.** (1986) Carbon dioxide and organic acids: their role in porosity enhancement and cementation, Paleogene of the Texas Gulf Coast. In: *Roles of Organic Matter in Sediment Diagenesis* (Ed. D.L. Gautier), *SEPM Spec. Publ.*, **38**, 129–146.

Machel, H. (2001) Bacterial and thermochemical sulfate reduction in diagenetic settings – old and new insights. *Sed. Geol.*, **140**, 143–175.

Maliva, R.G., **Knoll, A.H.** and **Simonson, B.M.** (2005) Secular change in the Precambrian silica cycle: insights from chert petrology. *Geol. Soc. Am. Bull.*, **117**, 835–845.

Maliva, R.G., **Budd, D.A.**, **Clayton, E.A.**, **Missimer, T.M.** and **Dickson, J.D.** (2011) Insights into the dolomitization process and porosity modification in sucrosic dolostones, Avon Park Formation (Middle Eocene), East-Central Florida, U.S.A. *J. Sed. Res.*, **81**, 218–232.

Maloof, A.C., **Ramezani, J.**, **Bowring, S.A.**, **Fike, D.A.**, **Porter, S.M.** and **Mazouad, M.** (2010) Constraints on early Cambrian carbon cycling from the duration of the Nemakit-Daldynian–Tommotian boundary δ13C shift, Morocco. *Geology*, **38**, 623–626.

Martins-Neto, M.A. (2009) Sequence stratigraphic framework of Proterozoic successions in eastern Brazil. *Mar. Pet. Geol.*, **26**, 163–176.

Martins-Neto, M.A., **Pedrosa-Soares, A.C.** and **Lima, S.A.A.** (2001) Tectono-sedimentary evolution of sedimentary basins from Late Paleoproterozoic to Late Neoproterozoic in the São Francisco craton and Araçuaí fold belt, eastern Brazil. *Sed. Geol.*, **141–142**, 343–370.

Mazzullo, S.J. and **Harris, P.M.** (1991) An overview of dissolution porosity development in the deep-burial environment, with examples from carbonate reservoirs in the Permian Basin. In: *Permian Basin Plays–Tomorrow's Technology Today* (Ed. M. Candelaria), *W. Tex. Geol. Soc. Publ.*, **91–89**, 125–138.

Mazzullo, J., **Sims, D.** and **Cunningham, D.** (1986) The effects of eolian sorting and abrasion upon the shapes of fine quartz sand grains. *J. Sed. Res.*, **56**, 45–56.

Miller, J.A. (1975) Facies characteristics of Laguna Madre Wind-Tidal Flats. In: *Tidal Deposits* (Ed. R.N.L. Ginsburg), pp. 67–72. Springer, New York.

Mills, M.M., **Ridame, C.**, **Davey, M.**, **La Roche, J.** and **Geider, R.J.** (2004) Iron and phosphorus co-limit nitrogen fixation in the eastern tropical North Atlantic. *Nature*, **429**, 292–294.

Misi, A. and **Kyle, J.R.** (1994) Upper Proterozoic carbonate stratigraphy, diagenesis, and stromatolitic phosphorite formation, Irecê Basin, Bahia, Brazil. *J. Sed. Res.*, **64**, 299–310.

Misi, A. and **Veizer, J.** (1998) Neoproterozoic carbonate sequences of the Una Group, Irecê Basin, Brazil: chemostratigraphy, age and correlations. *Precambrian Res.*, **89**, 87–100.

Misi, A., **Kaufman, A.J.**, **Veizer, J.**, **Powis, K.**, **Azmy, K.**, **Boggiani, P.C.**, **Gaucher, C.**, **Teixeira, J.B.G.**, **Sanches, A.L.** and **Iyer, S.S.S.** (2007) Chemostratigraphic correlation of Neoproterozoic successions in South America. *Chem. Geol.*, **237**, 143–167.

Mitchell, R.H. (2014) Chapter 8: Cathodoluminescence of Apatite. In: *Cathodoluminescence and its Application to Geoscience* (Ed. I.M. Coulson) Short Course Series Volume 45, pp. 143–167. Mineral Association of Canada (MAC), Québec, Canada.

Morad, S., **Marfil, R.**, **Al-Aasm, I.S.** and **Gomez-Gras, D.** (1992) The role of mixing-zone dolomitization in sandstone cementation: evidence from the Triassic Buntsandstein, the Iberian Range, Spain. *Sed. Geol.*, **80**, 53–65.

Mount, J.F. and **McDonald, C.** (1992) Influence of changes in climate, sea level, and depositional systems on the fossil record of the Neoproterozoic-Early Cambrian metazoan radiation, Australia. *Geology*, **20**, 1031–1034.

Narbonne, G.M. (1998) The Ediacara biota: a terminal Neoproterozoic experiment in the evolution of life. *GSA Today*, **8**, 1–6.

Narbonne, G.M. (2005) The Ediacaran Biota: neoproterozoic origin of animals and their ecosystems. *Annu. Rev. Earth Planet. Sci.*, **33**, 421–442.

Narbonne, G.M. (2010) Ocean chemistry and early animals. *Science*, **328**, 53–54.

Nelson, G.J., **Pufahl, P.K.** and **Hiatt, E.E.** (2010) Paleoceanographic constraints on Precambrian phosphorite accumulation, Baraga Group, Michigan, USA. *Sed. Geol.*, **226**, 9–21.

Nriagu, J.O. (1976) Phosphate-clay mineral relations in soils and sediments. *Can. J. Earth Sci.*, **13**, 717–736.

Och, L.M. and **Shields-Zhou, G.A.** (2012) The Neoproterozoic oxygenation event: environmental perturbations and biogeochemical cycling. *Earth Sci. Rev.*, **110**, 26–57.

Papineau, D. (2010) Global biogeochemical changes at both ends of the Proterozoic: insights from phosphorites. *Astrobiology*, **10**, 165–181.

Papineau, D., **Purohit, R.**, **Fogel, M.L.** and **Shields-Zhou, G.A.** (2013) High phosphate availability as a possible cause for massive cyanobacterial production of oxygen in the Paleoproterozoic atmosphere. *Earth Planet. Sci. Lett.*, **362**, 225–236.

Pedrosa-Soares, A., **Noce, C.**, **Wiedemann, C.** and **Pinto, C.** (2001) The Araçuaí-West-Congo Orogen in Brazil: an overview of a confined orogen formed during Gondwanaland assembly. *Precambrian Res.*, **110**, 307–323.

Pflug, R. and **Renger, F.E.** (1973) Estratigrafia e evolu\ccão geológica da margem SE do Cráton Sanfranciscano. In: *Congresso Brasileiro de Geologia*, pp. 5–19. Sociedade Brasileira de Geologia (SBG), Ribeirão Preto, Brazil.

Pimentel, M.M., **Fuck, R.A.** and **Botelho, N.F.** (1999) Granites and the geodynamic history of the Neoproterozoic Brasilia belt, Central Brazil: a review. *Lithos*, **46**, 463–483.

Planavsky, N.J., **Rouxel, O.J.**, **Bekker, A.**, **Lalonde, S.V.**, **Konhauser, K.O.**, **Reinhard, C.T.** and **Lyons, T.W.** (2010) The evolution of the marine phosphate reservoir. *Nature*, **467**, 1088–1090.

Plint, A.G. (2010) Wave-and storm-dominated shoreline and shallow-marine systems. In: *Facies Models 4* (Eds N.P. James and R.W. Dalrymple), 4th edn, pp. 167–200. Geological Association of Canada, St. John's, Canada.

Porter, K.G. and **Robbins, E.I.** (1981) Zooplankton fecal pellets link fossil fuel and phosphate deposits. *Science*, **212**, 931–933.

Porter, S.M., **Knoll, A.H.** and **Affaton, P.** (2004) Chemostratigraphy of Neoproterozoic cap carbonates from the Volta Basin, West Africa. *Precambrian Res.*, **130**, 99–112.

Poulton, S.W., **Fralick, P.W.** and **Canfield, D.E.** (2004) The transition to a sulphidic ocean ~1.84 billion years ago. *Nature*, **431**, 173–177.

Poulton, S.W., **Fralick, P.W.** and **Canfield, D.E.** (2010) Spatial variability in oceanic redox structure 1.8 billion years ago. *Nat. Geosci.*, **3**, 486–490.

Powell, C.M. and **Pisarevsky, S.A.** (2002) Late Neoproterozoic assembly of East Gondwana. *Geology*, **30**, 3–6.

Pufahl, P.K. (2010) Bioelemental sediments. In: *Facies Models 4* (Eds N.P. James and R.W. Dalrymple), 4th edn, pp. 477–504. Geological Association of Canada, St. John's, Canada.

Pufahl, P.K. and **Hiatt, E.E.** (2012) Oxygenation of the Earth's atmosphere–ocean system: a review of physical and chemical sedimentologic responses. *Mar. Pet. Geol.*, **32**, 1–20.

Pufahl, P.K., **Grimm, K.A.**, **Abed, A.M.** and **Sadaqah, R.M.** (2003) Upper Cretaceous (Campanian) phosphorites in Jordan: implications for the formation of a south Tethyan phosphorite giant. *Sed. Geol.*, **161**, 175–205.

Reddy, S.M. and **Evans, D.A.D.** (2009) Palaeoproterozoic supercontinents and global evolution: correlations from core to atmosphere. In: *Palaeoproterozoic Supercontinents and Global Evolution* (Eds S.M. Reddy, R. Mazumder, D.A.D. Evans and A.S. Collins), *Geol. Soc. London. Spec. Publ.*, **323**, 1–26.

Reineck, H.-E. and **Singh, I.B.** (1980) Tidal flats. In: *Depositional Sedimentary Environments: With Reference to Terrigenous Clastics* (Eds H.-E. Reineck and I.B. Singh), 2nd edn, pp. 430–456. Springer-Verlag, Berlin.

Rodrigues, J.B. (2008) *Proveniência de sedimentos dos grupos Canastra, Ibiá, Vazante e Bambuí–Um estudo de zircões detríticos e Idades Modelo Sm-Nd.* Unpublished PhD Dissertation, Instituto de Geociências, Universidade de Brasília, Brazil.

Romeiro Silva, P.C. (1997) A passagem do Mesoproterozóico para o Neoproterozóico no centro-leste do Brasil eo estilo estrutural envolvido. *Boi. Soe. Brás. Geol. Núcleo Minas Gerais*, **14**, 9.

Schulz, H.N. and **Schulz, H.D.** (2005) Large Sulfur Bacteria and the Formation of Phosphorite. *Science*, **307**, 416–418.

Schwartz, R.K. (1982) Bedform and stratification characteristics of some modern small-scale washover sand bodies. *Sedimentology*, **29**, 835–849.

Segonzac, G.D. (1970) The transformation of clay minerals during diagenesis and low-grade metamorphism: a review. *Sedimentology*, **15**, 281–346.

She, Z., **Strother, P.**, **McMahon, G.**, **Nittler, L.R.**, **Wand, J.**, **Zhang, J.**, **Sang, L.**, **Ma, C.** and **Papineau, D.** (2013) Terminal Proterozoic cyanobacterial blooms and phosphogenesis documented by the Doushantuo granular phosphorites I: *in situ* microanalysis of textures and composition. *Precambrian Res.*, **235**, 20–35.

Shen, Y., **Zhang, T.** and **Hoffman, P.F.** (2008) On the coevolution of Ediacaran oceans and animals. *Proc. Natl Acad. Sci. USA*, **105**, 7376–7381.

Sherman, A.G., **James, N.P.** and **Narbonne, G.M.** (2000) Sedimentology of a late Mesoproterozoic muddy carbonate ramp, northern Baffin Island, Arctic Canada. In: *Carbonate Sedimentation and Diagenesis in the Evolving Precambrian World* (Eds J.P. Grotzinger and N.P. James), *SEPM Spec. Publ.*, **67**, 275–294.

Shields, G.A. (2007) A normalised seawater strontium isotope curve: possible implications for Neoproterozoic-Cambrian weathering rates and the further oxygenation of the Earth. *eEarth*, **2**, 35–42.

Shields, G., **Stille, P.** and **Brasier, M.D.** (1999) Isotopic records across two phosphorite giant episodes compared: the Precambrian-Cambrian and the late Cretaceous-recent. In: *Marine Authigenesis: From Global to Microbial* (Eds C.R. Glenn, L. Prévôt-Lucas and J. Lucas), *SEPM Spec. Publ.*, **66**, 103–116.

Shields, G., **Kimura, H.**, **Yang, J.** and **Gammon, P.** (2004) Sulphur isotopic evolution of Neoproterozoic-Cambrian seawater: new francolite-bound sulphate δ34S data and a

critical appraisal of the existing record. *Chem. Geol.*, **204**, 163–182.

Shields-Zhou, G. and **Och, L.** (2011) The case for a neoproterozoic oxygenation event: geochemical evidence and biological consequences. *GSA Today*, **21**, 4–11.

Sial, A.N., **Dardenne, M.A.**, **Misi, A.**, **Pedreira, A.J.**, **Gaucher, C.**, **Ferreira, V.P.**, **Silva Filho, M.A.**, **Uhlein, A.**, **Pedrosa-Soares, A.C.** and **Santos, R.V.** (2009) The São Francisco Palaeocontinent. *Dev. Precambrian Geol.*, **16**, 31–69.

Sibley, D.F. and **Gregg, J.M.** (1987) Classification of dolomite rock textures. *J. Sed. Res.*, **57**, 967–975.

Smale, D. (1973) Silcretes and associated silica diagenesis in southern Africa and Australia. *J. Sed. Res.*, **43**, 1077–1089.

Solomon, S.T. and **Walkden, G.M.** (1985) The application of cathodoluminescence to interpreting the diagenesis of an ancient calcrete profile. *Sedimentology*, **32**, 877–896.

Soudry, D. (2000) Microbial phosphate sediment. In: *Microbial Sediments* (Eds R.E. Riding and S.N. Awramik), pp. 127–136. Springer, Berlin, Heidelberg.

Southgate, P.N. (1986) Cambrian phoscrete profiles, coated grains, and microbial processes in phosphogenesis; Georgina Basin, Australia. *J. Sed. Res.*, **56**, 429–441.

Sperling, E.A., **Pisani, D.** and **Peterson, K.J.** (2007) Poriferan paraphyly and its implications for Precambrian palaeobiology. *Geol. Soc. London. Spec. Publ.*, **286**, 355–368.

Sperling, E.A., **Peterson, K.J.** and **Laflamme, M.** (2011) Rangeomorphs, Thectardis (Porifera?) and dissolved organic carbon in the Ediacaran oceans. *Geobiology*, **9**, 24–33.

Trappe, J. (2001) A nomenclature system for granular phosphate rocks according to depositional texture. *Sed. Geol.*, **145**, 135–150.

Trompette, R., **Affaton, P.**, **Joulia, F.** and **Marchand, J.** (1980) Stratigraphic and structural controls of late Precambrian phosphate deposits of the northern Volta Basin in Upper Volta, Niger, and Benin, West Africa. *Econ. Geol.*, **75**, 62–70.

Tucker, M. (1982) Storm-surge sandstones and the deposition of interbedded limestone: Late Precambrian, southern Norway. In: *Cyclic and Event Stratification* (Eds G. Einsele and A. Seilacher), pp. 363–370. Springer, Berlin, Heidelberg.

Van Cappellen, P. and **Ingall, E.D.** (1994) Benthic phosphorus regeneration, net primary production, and ocean anoxia: a model of the coupled marine biogeochemical cycles of carbon and phosphorus. *Paleoceanography*, **9**, 677–692.

Van Cappellen, P. and **Ingall, E.D.** (1996) Redox stabilization of the atmosphere and oceans by phosphorus-limited marine productivity. *Science*, **271**, 493–496.

Vandenberghe, J. (2013) Grain size of fine-grained windblown sediment: a powerful proxy for process identification. *Earth Sci. Rev.*, **121**, 18–30.

Vieillard, P. and **Tardy, Y.** (1984) Thermochemical properties of phosphates. In: *Phosphate Minerals* (Eds D.J.O. Nriagu and P.B. Moore), pp. 171–198. Springer, Berlin, Heidelberg.

Walker, D.I. (1985) Correlations between salinity and growth of the seagrass *Amphibolis antarctica* (Labill.) Sonder & Aschers., In Shark Bay, Western Australia, using a new method for measuring production rate. *Aquat. Bot.*, **23**, 13–26.

Wallmann, K. (2003) Feedbacks between oceanic redox states and marine productivity: a model perspective focused on benthic phosphorus cycling. *Global Biogeochem. Cycles*, **17**, 1084.

Wang, X., **Zhang, L.**, **Zhang, H.**, **Wu, X.** and **Mei, D.** (2012) Phosphorus adsorption characteristics at the sediment–water interface and relationship with sediment properties in FUSHI reservoir, China. *Environ. Earth Sci.*, **67**, 15–22.

Windom, H.L. (1975) Eolian contributions to marine sediments. *J. Sed. Res.*, **45**, 520–529.

Wright, V.P. and **Burchette, T.P.** (1998) Carbonate ramps: an introduction. *Geol. Soc. London. Spec. Publ.*, **149**, 1–5.

Xiao, S. and **Laflamme, M.** (2009) On the eve of animal radiation: phylogeny, ecology and evolution of the Ediacara biota. *Trends Ecol. Evol.*, **24**, 31–40.

Xiao, S., **Zhang, Y.** and **Knoll, A.H.** (1998) Three-dimensional preservation of algae and animal embryos in a Neoproterozoic phosphorite. *Nature*, **391**, 553–558.

Yueyan, L., **Cook, P.J.** and **Shergold, J.H.** (1986) Proterozoic and Cambrian phosphorites—regional review: China. In: *Phosphate Deposits of the World, Volume 1, Proterozoic and Cambrian Phosphorites* (Eds P.J. Cook and J.H. Shergold), pp. 42–62. Cambridge University Press, Cambridge.

Zentmyer, R.A., **Pufahl, P.K.**, **James, N.P.** and **Hiatt, E.E.** (2011) Dolomitization on an evaporitic Paleoproterozoic ramp: widespread synsedimentary dolomite in the Denault Formation, Labrador Trough, Canada. *Sed. Geol.*, **238**, 116–131.

Zhang, X., **Shu, D.**, **Han, J.**, **Zhang, Z.**, **Liu, J.** and **Fu, D.** (2014) Triggers for the Cambrian explosion: hypotheses and problems. *Gondwana Res.*, **25**, 896–909.

Manuscript received 17 October 2014; revision accepted 8 May 2015